COMPARATIVE STUDY OF GRAPHENE-BASED STRUCTURAL ELECTRODES

A Thesis

by

SAEROM YU

Submitted to the Office of Graduate and Professional Studies of
Texas A&M University
in partial fulfillment of the requirements for the degree of

MASTER OF SCIENCE

Chair of Committee,	Micah Green
Committee Members,	Jodie Lutkenhaus
	James Boyd
Head of Department,	Efstratios Pistikopoulos

August 2018

Major Subject: Energy

ABSTRACT

Graphene based electrodes have gained significant attention in the field of high-performance energy devices. Among different types of graphene-electrode assemblies, our team chose to approach 3D gel morphology due to its high specific surface area, and high porosity. We prepared graphene hydrogels by controlled reduction-led self-assembly of graphene oxide nanosheets in presence of ammonia. Our recent approach considers aramid nanofibers as fillers for mechanical enhancement in 3D graphene oxide hydrogels based electrodes. Several characterization techniques are discussed to measure the mechanical and electrochemical properties of electrodes. These performance metrics can be used to compare the performance of gel based electrodes with other electrodes types. To get an in-depth understanding of how graphene architecture affects the electrode performance and to determine what factors give rise to better performing structural electrode, several literatures are reviewed as a comparative study.

DEDICATION

This thesis is dedicated to my parents (Jaedeok Yu, Sukkyung Park) and sisters and brother (Eunseon Yu, Juseon Yu, Euijin Yu, Sujin Yu, Jihee Yu) as my great supporters. It is their education and embracing love throughout my life that taught me to be passionate with what I do, put efforts on it, and be patient. I will treasure them deep in my heart.

I would like to thank to members of Green Group. Big gratitude to my advisor Dr. Green, for all his support, guidance and insight enriching my learning throughout this work. Big thanks to Shah Smit, for his encouragement and help.

CONTRIBUTORS AND FUNDING SOURCES

Contributors

This thesis was supervised by a thesis committee consisting of Professor Micah Green and Jodie Lutkenhaus of the Artie McFerrin Department of Chemical Engineering and Professor James Boyd of the Department of Aerospace Engineering.

The data analyzed for Section 5 was and provided by Shah Smit.

Funding Sources

Graduate study was supported by a scholarship from Engineering Development Research Center.

NOMENCLATURE

E	Young's modulus
EDLC	electric double layer capacitor
ESR	equivalent series resistance
GA	graphene aerogel
GH	graphene hydrogel
GO	graphene oxide
rGO	reduced graphene oxide
3D	three-dimensional

TABLE OF CONTENTS

Page

ABSTRACT ii

DEDICATION iii

CONTRIBUTORS AND FUNDING SOURCES iv

NOMENCLATURE v

TABLE OF CONTENTS vi

LIST OF FIGURES vii

1. INTRODUCTION 1
   1.1. Motivation 1
   1.2. Background on battery and supercapacitor technology 2
   1.3. Background on processing of graphene-based materials 6

2. PRIOR WORK ON CARBON-BASED ELECTRODES 12
   2.1. Carbon-based electrodes 12
   2.2. Graphene-based electrodes 14
   2.3. Structural electrodes 14

3. GRAPHENE MATERIAL ARCHITECTURES FOR ELECTRODE USAGE 21
   3.1. Compressed powder as conventional electrode 21
   3.2. Graphene gel-based electrode 22
      3.2.1. Preparation of graphene hydrogels 22
      3.2.2. Preparation of graphene aerogels 24

4. PERFORMANCE METRICS FOR STRUCTURAL ELECTRODES 26
   4.1. Background of characterization technique 26
      4.1.1. Characterizing mechanical properties of hydrogel (wet) 26
      4.1.2. Characterizing mechanical properties of powder (dry) 30
      4.1.3. Electrochemical properties 34

5. OUR EXPERIMENT AND RESULTS SO FAR 39

6. SUMMARIES OF LITERATURE REVIEW AND COMPARISON: ASSESSING PROPERTIES OF MULTIFUNCTIONAL ELECTRODE MATERIALS 42

7. CONCLUSION 57

REFERENCES 59

APPENDIX 67

LIST OF FIGURES

Page

Figure 1 Schematic illustration of the charging and discharging process in a supercapacitor 4

Figure 2 Ragone plot of electrochemical energy storage/conversion systems 6

Figure 3 Schematic of top-down graphene synthesis approach 8

Figure 4 Phase diagram illustrating top-down approaches to prepare graphene 9

Figure 5 Hierarchical structure of fiber reinforced composite with different levels of length 16

Figure 6 Illustration of a structural supercapacitor in laminated architecture using conductive carbon fiber weaves as electrodes and glass fiber weaves as separators 17

Figure 7 Comparison of CNT fibers and carbon fibers 19

Figure 8 Schematic of sol-gel rGO gels synthesis 23

Figure 9 Phase diagram of water illustrating different drying routes with plotted pressure and temperature 25

Figure 10 Schematic of mechanical characterization methods of hydrogels 27

Figure 11 A comparison between the use of dynamic mechanical analysis and oscillatory shear rheometry for mechanical characterization of hydrogels 29

Figure 12 Schematic of peel test, and drag test 32

Figure 13 Conceptual drawing of bending deformation involving compressive and tensile strains 34

Figure 14 Galvanostatic charge/discharge curves and CV curve of supercapacitors 37

Figure 15 GO gel/H_2SO_4/GO gel symmetric coin cell used for supercapacitor device testing . 38

Figure 16 Rheology test for mechanical characterization of GO/ANF hydrogels 40

Figure 17 Mechanical Properties of GO/ANF Gels with different ANF content 41

Figure 18 Comparison of electrochemical properties of nitrogen/phosphorus co-doped graphene monolith and conventional powder electrode 44

Figure 19 Schematic illustration depicting different mechanical behaviors of GO paper on bending test and tensile test 46

Figure 20 Electrochemical performances of rGO films 48

Figure 21 Ashby plot showing comparison of rGO/ANF composite against free-standing paper electrodes 49

Figure 22 Electrochemical behavior and mechanical behavior of graphene hydrogels prepared by hydrothermal method 53

Figure 23 Images of graphene hydrogels with different ammonia content 55

1. INTRODUCTION

1.1. Motivation

Today, demand for energy storage devices is increasing for use in highly efficient electric or hybrid vehicles, weight saving in aircrafts, and portable electronic equipment. In these applications, energy devices have important roles since they require high specific energy and power. While studies on energy storage systems have been actively investigating to develop high-performance electrode materials and evaluate electrochemical properties that can replace conventional electrode materials, there are still many challenges to commercialize. Our interest lies in developing novel electrode materials, especially, by producing multifunctional materials that serve not only as active materials for storing energy but also as structural components in applications. Such multifunctional-electrode materials are well known as “structural electrodes”. One can design a structural electrode to get a desirable combination of these two properties to address a target application. Usually, there is a trade-off between the mechanical and electrochemical properties in a multifunctional material. There are several factors that control mechanical properties, energy storage, and their trade-offs, such as architecture, composition, functional groups, crosslinks, and interfaces among which architecture is focused in this project. Specifically, graphene hydrogel-based electrodes as 3D open porous monolithic architecture are evaluated against dry gel electrodes against powder and paper types of electrodes. Metrics for measuring electrochemical and mechanical performance of these structures are also discussed. Generally, studies related to graphene gel-based electrodes emphasize on electrochemical performances while mechanical

properties are rarely reported. In contrast, studies emphasizing mechanical properties of gel-based structures, rarely report electrochemical properties. Due to this issue, it is crucial to find advantageous and disadvantageous features of each electrode types as comparison since these features satisfy different application, which is addressed in this project.

1.2. Background on battery and supercapacitor technology

Batteries and supercapacitors are commonly used energy storage devices. Batteries are known for high energy density and they transform chemical energy into electrical energy through reduction and oxidation reactions. Lithium-ion batteries are commonly used for electronics like smartphones and laptops. There are three major parts in batteries: cathode, anode, and electrolyte.[25] Anode is the electropositive electrode. During discharge, lithium ions in an electrolyte are intercalated between layers of conducting anode electrode where electrons are originated from reaction. Reduction occurs when generated electrons are sent to the cathode. Cathode, which is the electronegative electrode, accepts electrons (oxidation) from the anode through external circuit connected to current collectors that are typically metals adhering to electrode material without reacting with electrode. Lithium ions travel through the electrolyte from anode to cathode while electrons move. During the charge step of the battery, lithium ions and electrons move in the opposite direction. Batteries face several challenges such as relatively slow charging and discharging process and short life span (1000 charge and discharge cycles). This is because electrode materials

are damaged by mechanical expansion and contraction from electrolyte intercalation as they go through charge and discharge cycles.[27]

Supercapacitors are known for their capability for rapid and reversible charge and discharge process, longer life, high power density, but, lower energy density compared to batteries.[12,29,30] Low energy contents of supercapacitors are resulted from the fact that chemical reactions are not involved in supercapacitors.[31] However, they rapidly respond to potential changes, contributing to high power density. There are two types of supercapacitors: electric double layer capacitor (EDLC) and pseudocapacitor. EDLC is composed of two electrodes, a separator and an electrolyte. Generation of electricity is a consequence of the movement of ions or reaction at the interfaces of electrolyte and electrode where charges are accumulated (Figure 1: a, b) forming electrical double layers (EDLs) during charging.[12] During discharging, EDLs are released. Energy is delivered by electrons moving through external wire connected to current collector. Since EDLC does not cause damage to the electrodes, their charge-discharge cycling performance is much better than batteries, increasing their lifetime. Furthermore, since time for charging and discharging is short, it is possible to perform fast energy transfer in a short period of time. Therefore, EDLCs are useful when high power is necessary, while energy storage capacity needs to be improved. This can be achieved by using advanced electrode with high specific surface area, large pore sizes and conductive materials.

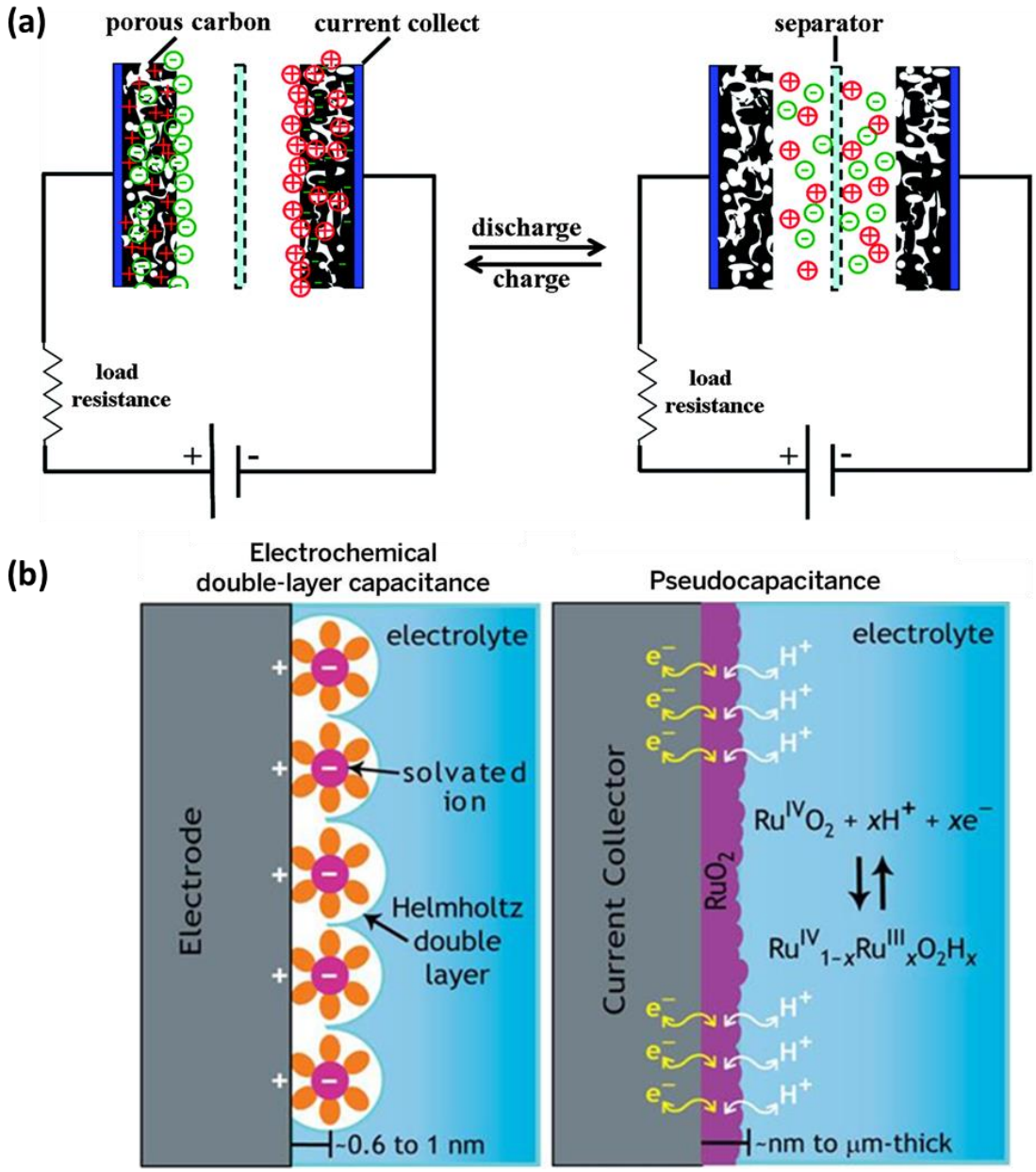

Figure 1: Schematic illustration of the charging and discharging process in a supercapacitor. (a) Charge is formed at electrode/electrolyte interface as electric double layers. Reprinted from ref. [10] (b, left) Conceptual drawing of mechanisms of EDLC, and (b, right) pseudocapacitors. Reprinted with permission from ref. [2]

A pseudocapacitor is a component of an electrochemical capacitor with conductive materials or metal oxides such as VO, MnO_2 or RuO_2 as electrode materials. Unlike EDLC, it involves a chemical reaction to overcome low energy density resulting from electrostatic interaction. Thus, fast and reversible reduction-oxidation reactions (redox reactions) at the surface or subsurface of pseudo-capacitive materials influences pseudo-capacitance. The charge is transferred between electrode and electrolyte through adsorption process, redox reaction and intercalation of ions.[2] Figure 1 (b) depicts this; when the electrode (RuO_2) is negatively charged, unsolvated protons (H^+) in electrolyte are adsorbed on electrodes and redox reaction occurs; reduction occurs in the electrode and gives rise to $Ru(OH)_2$. Then, with the charge removed, reaction occurs reversely in the electrode; protons are emitted to electrolytes and electrons are transferred to current collector. This leads to an increase in capacitance (energy density) at the cost of power density and cyclability.[33-35]

In most existing energy storage systems, either energy or power performance is sacrificed, as presented in (Figure 2). To get specific energy, specific power is relatively poor, and vice versa. To deal with this trade-off, there have been many dedicated efforts to obtain superior energy and power performances by exploring composite or hybrid electrode materials. These electrodes performances are indicated by overlapping area between batteries and supercapacitors in Figure 2.[12]

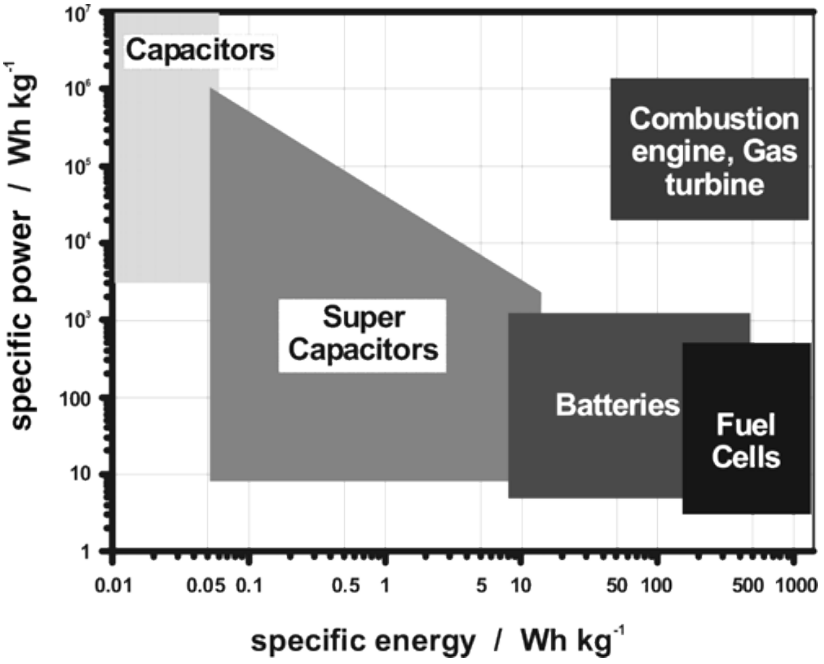

Figure 2: Ragone plot of electrochemical energy storage/conversion systems; horizontal axis is specific energy (Wh/kg) and vertical axis is specific power (W/kg). Batteries show specific energy (~400 Wh/kg) while specific power value is low (~1000 W/kg). Supercapacitors show low specific energy (~10 Wh/kg) but high specific power (~10000 W/kg). Reprinted with permission from ref.[12]

1.3. Background on processing of graphene-based materials

Graphene is an attractive material for use in electrodes. Graphene is a sp^2-hybridized carbon atomic layer, and has excellent mechanical and electrochemical properties such as high electron mobility, high specific surface area ($2630 m^2 g^{-1}$),[36] high thermal conductivity ($4.84\times10^3 - 5.30\times10^3$ $W\cdot m^{-1}\cdot K^{-1}$),[37] and high mechanical strength (1

TPa) for a single layer of graphene.[38] Specific capacitance of a graphene layer reaches 21 μF cm^{-2}, if there is no wasted surface.[39] To prepare graphene, bottom-up and top-down approaches are considered.

In bottom-up approach, there are several strategies including epitaxial growth, and chemical vapor deposition (CVD). CVD can be used to produce graphene structure on a substrate such a SiC and metal surfaces exposed to gaseous hydrocarbon precursors, such as methane, ethylene, and acetylene at high temperature.[40,41] On a large-area, the growth of carbon atoms starts with nucleation after decomposition of the hydrocarbons and nuclei growth. CVD employs plasma-enhanced CVD, thermal CVD, or hot/cold wall CVD. Typically, the resulting graphene is high quality and can cover large area. One of the common synthesis method is to use nickel foam as sacrificial template so that graphene is formulated based on the structure via CVD. Another bottom-up approach is pyrolysis of carbon precursor such as methane or PMMA. However, even though bottom-up approaches offer growth of graphene in a large-area and controllable synthesis, they face challenges of mass production and cost-effectiveness.

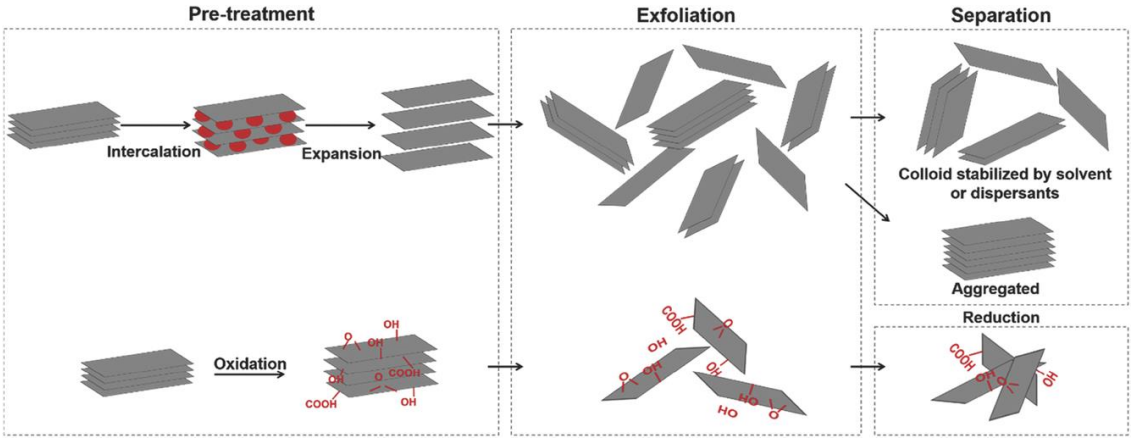

Figure 3: Schematic of top-down graphene synthesis approach involving three steps: pre-treatment, exfoliation, and separation. Reprinted with permission from ref.[13]

Top-down approaches refer to the processing of bulk materials (graphite) into nano-size materials (graphene). Graphite exists as stacked graphene layers connected by attractive interlayer van der Waals forces. To separate graphene layers, another driving force such as mechanical forces or chemical functionalization is required to address van der Waals forces. Followed by this, exfoliated graphene nanosheets need liquid medium to maintain its exfoliated formation.[13] This liquid phase is mostly dispersant or surfactant. For processing graphene, typical steps employed are pretreatment, exfoliation, separation, and/or reduction, depicted in Figure 3. A widely used physical method involves pre-treatment that intercalates of graphite with small molecules, followed by thermal expansion, resulting in formation of expanded graphite. This form of graphite has increased interlayer spaces, making it easier for the subsequent exfoliation step.

There are two main routes (as described in Figure 4) to obtain pristine graphene from graphite. First route is modified Hummers' method, which involves synthesis of graphene oxide (GO), and its subsequent reduction to obtain reduced graphene oxide (rGO). Second route involves mechanical exfoliation pathway to directly produce pristine graphene.

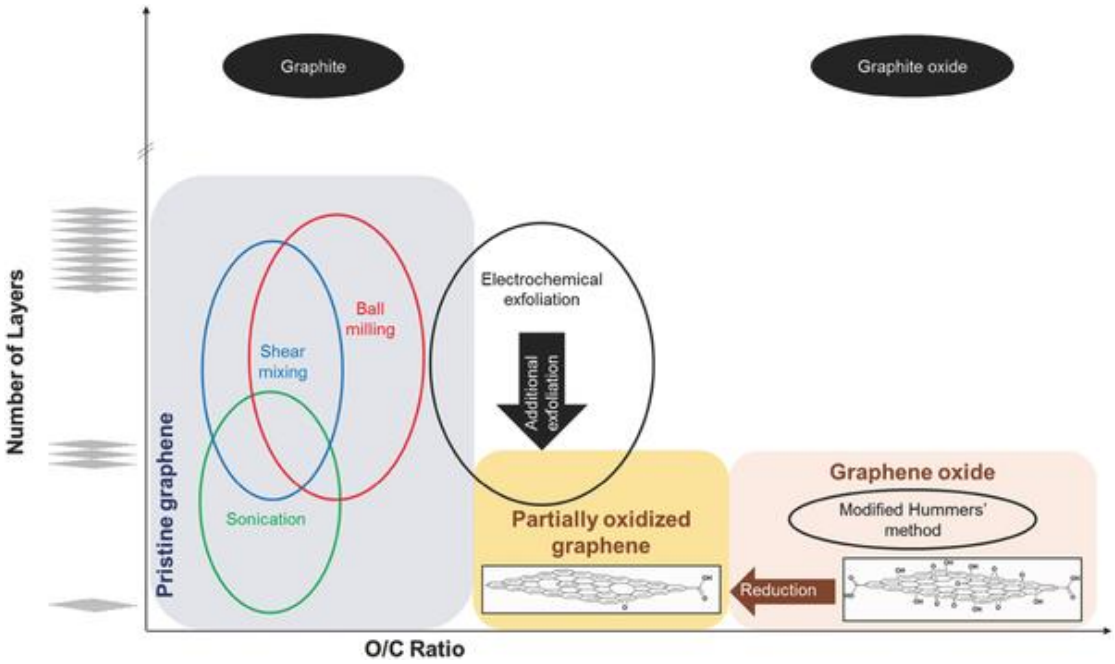

Figure 4: Phase diagram illustrating top-down approaches to prepare graphene as a function of oxidation degree and the number of layers. Reprinted with permission from ref.[13]

In modified Hummers' method, oxidized graphite produced through liquid-phase pretreatment is chemically exfoliated into GO in a functionalized form. This process occurs in presence of oxidants, such as sulfuric acid, nitric acid and potassium permanganate, inducing hydroxyl (-OH), carboxyl (-COOH), epoxide (-O-), and carbonyl

(C=O) functional groups.[42,43] As a result, hydrophilic GO nanosheets are obtained, which can form stable aqueous colloidal dispersions. The subsequent reduction step is required to restore sp^2 domain and electrical conductivity and is facilitated by reducing agents including hydrazine,[44] sodium borohydride,[45] and hydroquinine.[46] Depending on the reducing agent used and reaction pathway, the final reduced graphene oxide (rGO) nanosheets exhibit different characteristics.[47] For instance, number of constituent layers, lateral size, morphology influences properties of the resultant rGO sheet. Since original material is functionalized, properties of rGO are unavoidably sacrificed. Despite these issues, modified Hummers' method is still a common method to get graphene family materials.

In the mechanical exfoliation approach, three steps are employed: 1) exfoliation of graphite, 2) stabilization of graphene layers, and 3) separation of exfoliated graphene nanosheets from unexfoliated graphitic materials.[48] Mechanical exfoliation is achieved by sonication, shear mixing, and ball-milling. These exfoliation techniques are performed in either solid state or in a liquid medium where separation of graphene nanosheets occurs by means of overcoming interlayer van der Waals forces. Sonication and shear mixing are carried out in liquid phase, while ball-milling is carried out in solid-state. Liquid medium can either be an organic solvent or water with dispersant to prevent reaggregation. Ultrasonic waves induce cavitation in the solvent, which results in exfoliation of graphite.[49] However, long sonication time results in reduced lateral size of graphene nanosheets. In case of shear mixing, shear forces delaminate graphene nanosheets.[50]

Generally, compared to sonication, the produced graphene nanosheets have higher lateral size and less defects, but they have more layers.[51] Ball-milling is a well-known solid-state exfoliation technique that is advantageous for large-area and large-scale graphene production. This technique uses stainless steel balls to ball-milling graphite by applying shear force with assistance of gas mixtures or solvent. Followed by this, the milled mixture is washed with distilled water to remove defects and impurities on surface. However, excessive milling causes the basal plane distortion of obtained graphene.[52]

2. PRIOR WORK ON CARBON-BASED ELECTRODES

2.1. Carbon-based electrodes

Electrodes are usually complex composites. Components of conventional electrodes typically include active materials, binders, and conductive diluents.[53] Binders play an important role by supporting the powder structure but generally they have an insulating feature, which increases contact resistance between active materials when it is blended and lowers conductivity. To preserve conductivity, conductive diluents serve as providing the whole structure with electronic conductivity so that electrons are well transported to the active material.[54,55]

Carbons are widely used for electrodes since they can be fabricated into different structures such as fibers, thin films, powders and highly porous structures based on precursors.[56-63] For this reason, many carbon-based materials have been explored for electrode material including carbon-based composite, carbon black powder, carbon quantum dots, carbon nanotubes, carbon nanofibers, nitrogen-doped carbons, and graphene *etc*.[64] Carbon black is a product of incomplete combustion of hydrocarbon and works as active material as well as conductive additive in electrode.[65] Activated carbon is currently used supercapacitor electrode material manufactured from carbonaceous material such as wood, lignite coal, and coconut shell through a warm activation process with oxidizing agents.[66] Activation process is a conventional method to get desired porous structure, and the porosity is between 30~80%.[59,63,67] However, the obtained activated

carbon materials with highly porous structure is limited by poor mechanical performance. This has been compensated for using carbon-based nanomaterials in order to achieve a high porous structure with high mechanical strength, which is discussed in Section 5.

Carbon-based nanomaterials such as carbon nanotubes,[68] carbon aerogels, and graphene[7,18] are of interest because specific properties can be enhanced by their nanoscale dimensions, which allows high specific surface area and porous structure. Using these nanomaterials into electrode enables achieving high electrical conductivity and mechanical strength compared to electrodes composed of activated carbon materials.[64]

Many studies related with carbon electrodes for supercapacitors are directed towards forming carbon hybrid electrode with transition metal oxides (MnO_2, RuO_2, Fe_2O_4), hydroxides ($Ni(OH)_2$ and $Co(OH)_2$) or conductive polymers (PANI, polypyrroles and poly(3,4-ethylenedioxythiophene) to obtain higher capacitance owing to their charge storage mechanism. The produced materials are called ‘hybrid’ which is a mixture of more than two-phase material exhibiting pseudocapacitance. As an another approach, carbonaceous materials as a matrix for the electrode and combining it with functionalities or another component was identified to be a promising strategy to design multifunctional composite electrodes.[64]

2.2. Graphene-based electrodes

To investigate high performing supercapacitors, graphene-based materials have drawn tremendous interest as an alternative to activated carbon supercapacitors as another means to achieve decent energy density of supercapacitors. Specifically, for the use of electrode, graphene can be a useful material among the carbon family materials to get high charge accommodation and high conductivity due to its extraordinary electrical properties.[69] However, there is a restacking issue of graphene sheets that needs to be handled to maximize its surface area to achieve high energy and power performance. Graphene nanosheets assemblies in the form of quantum dots (0D), wires (1D), films (2D), monoliths (3D)[53] and adding spacers have been explored to minimize agglomeration. [38,70]

2.3. Structural electrodes

"Structural power technology" is known as an advanced technology in transport sector that involves transforming batteries into parts of the car, such as doors, hoods, and roofs. If properly implemented, this technology would bring achieving mass savings in electric vehicles with high battery dependence where light weight is an important challenge since its driving distance is proportional to battery performance.[71] Greenhalgh *et al.* described carbon-fiber body panels in electric vehicles serving as a battery or as a capacitor and reported that l5% of mass/volume saving is expected.[72] In order to achieve mass savings, many works on developing multifunctional composites as structural

material has been done. Multifunctional composite materials perform two functions: one function is related with energy management, and the other function is related with mechanical management. In this section, a multifunctional performance metric, and recent studies and challenge are discussed.

To assess whether structural materials can achieve mass savings, O'Brien *et al.* suggested a quantitative metric of multifunctionality by using efficiency factors.[73] η_e and η_s indicate electrical and mechanical efficiencies of multifunctional material, respectively. η_e can be expressed as ratio of electrical metric of multifuctional and conventional materials. η_s is expressed by ratio of specific moduli of multifuctional and conventional materials. If the summation of two efficiencies exceeds 1, we say that the multifunctional material renders savings in weight.

$$\eta_{\mathrm{mf}} \equiv \eta_e + \eta_s > 1 \quad \text{where} \quad \eta_e = \frac{\bar{\Gamma}_{mf}}{\bar{\Gamma}} \;\&\; \eta_s = \frac{\bar{E}_{mf}}{\bar{E}} \tag{1}$$

$\bar{\Gamma}_{mf}$ is an electrochemical property of multifunctional materials, and $\bar{\Gamma}$ is an electrochemical property of conventional materials. Energy density, power density, capacity, capacitance are used as electrochemical performance metrics. $\bar{E}_{mf}$ is a mechanical property of multifunctional materials. $\bar{E}$ is a mechanical property of conventional materials. Modulus, stiffness, strain-to-failure, ultimate strength, toughness are used as mechanical performance metrics.

As structural materials, fiber-reinforced composites (FRCs) with polymer-matrix has been developed in recent decades due to combination of low density, high stiffness, strength, and toughness.[3] By using the fiber infiltration with a polymeric matrix, existing issues has been tackled; there were several issues of fibrous materials, such as ultralow compressive strength of fibers owing to buckling behavior, and swift strength degradation owing to surface defects from environmental impact or permeable feature, and so on. There are hierarchical levels of resultant FRC structure according to their length scale: Ply, laminate and element.[3] At Ply level, matrix and fiber spatial arrangement and volume fraction are manipulated. At laminate level, stacking sequence and fiber architecture are controlled. Lastly, the spatial disposition of the laminates is considered at structural element level. Accordingly, properties of FRC can be adjusted at different levels due to its hierarchical structure (Figure 5).

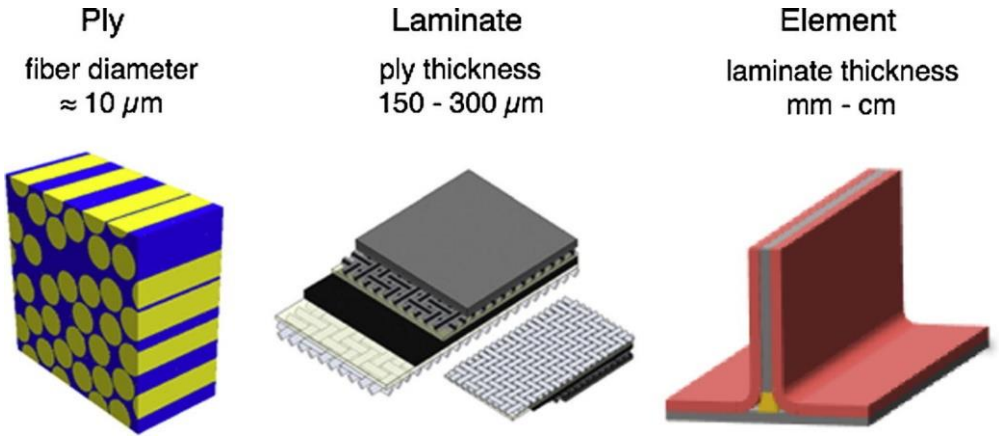

Figure 5. Hierarchical structure of fiber reinforced composite (FRC) with different levels of length. Reprinted with permission from ref.[3]

Sirshova *et al.* devised structural composite supercapacitors with laminated architecture.[15] The laminate composite working as a capacitor is made by combining woven carbon fiber layers with glass fiber layer. In an ion conducting matrix, the designed laminate composite material plays multifunction roles: carbon fiber layers function as electrodes and the glass fibers function as a separator. (Figure 6)

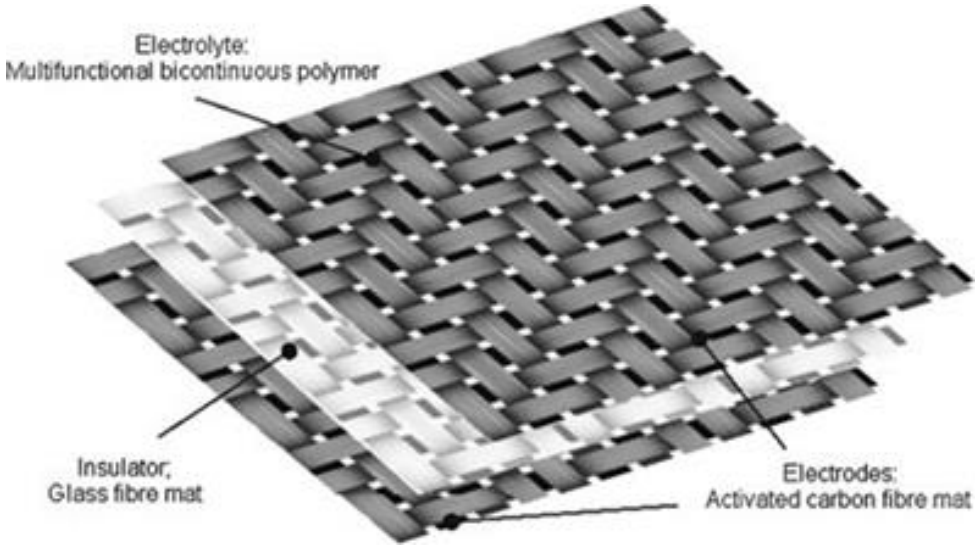

Figure 6: Illustration of a structural supercapacitor in laminated architecture using conductive carbon fiber weaves as electrodes and glass fiber weaves as a separator. Reprinted with permission from ref.[15]

González *et al*. pointed out one of major challenges of fiber-reinforced structural supercapacitors; reinforcing fiber is required to have high specific surface area unaccompanied by degradation of mechanical properties.[3] For instance, compared with CNT fibers, carbon fibers have relatively lower specific surface area and capacitance, while having higher stiffness and strength as indicated in Figure 7. CNT fibers are nanomaterials known for intrinsically large surface area (100 m^2/g), while carbon fibers have 0.2 m^2/g. Synder *et al.* performed electrochemical tests on structural carbon fibers existing in commercials and reported specific capacitance in a two-electrode coin cell with 1.0 M $LiPF_6$ at 20 mV/s.[74] The obtained capacitance was low, ranging from 0.4 to 3.5 F g^{-1}, which is attributed to low specific surface area while they have high stiffness (127~135 GPa/SG) and strength (2.2~2.4 GPa/SG). As a comparison, CNT fibers have relatively higher capacitance ranging from 23 to 79 F/g and lower stiffness (10~100 GPa/SG) and strength (0.15~2 GPa/SG).[23,26] In this context, there are current studies that try to combine carbon fibers and CNT fibers for making fiber-based structural electrode materials to achieve good electrochemical and mechanical performance. Electrochemical and mechanical properties of carbon-based electrodes are in the Appendix.

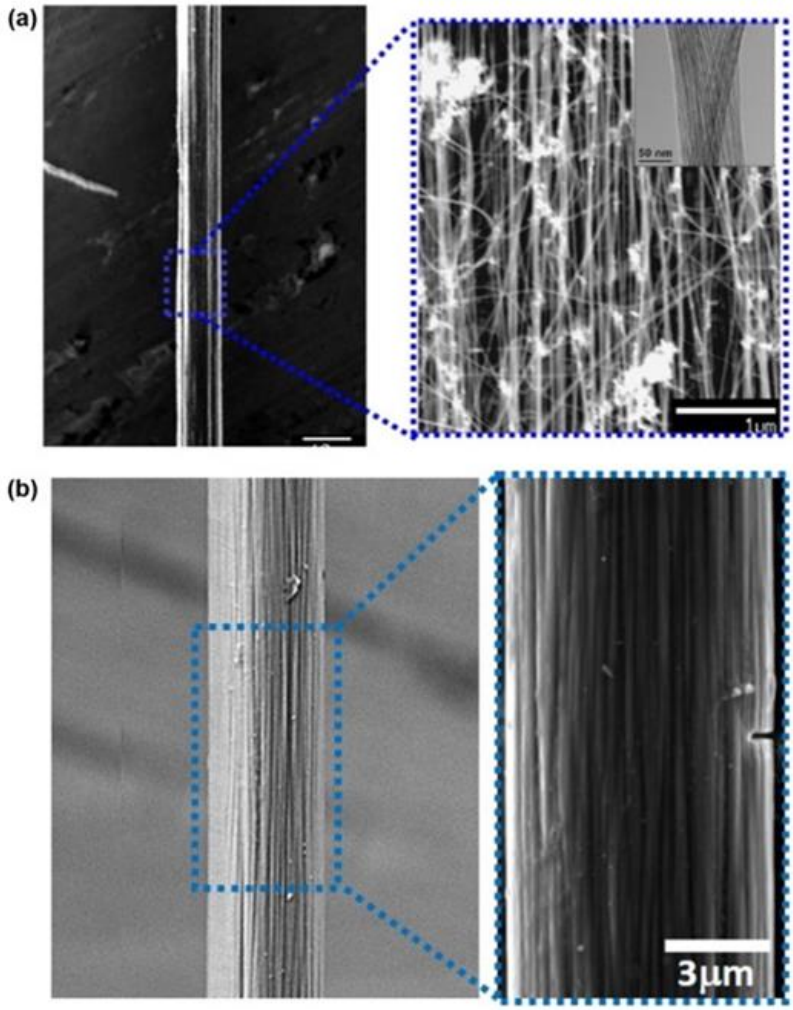

Figure 7: Comparison of CNT fibers and carbon fibers (a) CNT fibers with porous structure and high specific surface area. (b) carbon fibers with low specific surface area. Reprinted with permission from ref.[3]

Qian *et al*. made structural EDLC composite by modification that embeds woven carbon fiber fabrics in monolithic carbon aerogels.[5] Woven carbon fabric is impregnated in a resorcinol-formaldehyde polymer, and cured for 24 hours and at 50~90 ºC and then carbonized in a nitrogen atmosphere for 30 minutes at 800 ºC. The two carbon fabrics impregnated with carbon aerogels were sandwiched around separator to work as structural EDLC composite. They exhibit high specific surface area (160 m^2/g) and up to 4.5-fold increases in in-plane shear modulus (~5050 MPa) and strength (~26.2 MPa). Through electrochemical studies, the carbon fiber-monolithic carbon aerogel samples showed increase in capacitance from 0.06F/g to 5.9-14.3 F/g in 3M KCl at 5mV/s. These values are normalized by electrode material.

3. GRAPHENE MATERIAL ARCHITECTURES FOR ELECTRODE USAGE

3.1. Compressed powder as conventional electrode

In conventional electrodes, active materials are generally used in the form of nanoplatelets or nanopowders. The choice of binder determines the strength of an electrode; polyvinylidene fluoride (PVDF) and polytetrafluoroethylene (PTFE) are mostly used. Conductive diluents facilitate movement of electrons toward active material. To obtain a good mixture of these, organic solvents n-methyl-2-pyrrolidone (NMP) or dimethylformamide (DMF) are added to form a slurry.[75] This slurry is deposited onto the current collector. Then, it goes through drying and compression by mechanical force that determines the final density and porosity.

For coating techniques, there are doctor blading, bar coating, drop cast *etc*, among which doctor blading are commonly used. Blade moves to spread the slurry onto the substrate and thickness is controllable by adjusting the gap between substrate and the blade. In existing device, binder and additive accounts for 20~40% of the mass of the electrode for lab scale. Recent studies have been explored electrode materials that can be directly used and reduce components that are not conducive to energy storage performance. Especially, graphene assemblies are considered to give additional advantages such as offering various 3D structures, and controlling pore size and distribution.[55,76]

3.2. Graphene gel-based electrode

3.2.1. Preparation of graphene hydrogels

There are two solution-based reduction routes where GO is assembled: hydrothermal reduction and chemical reduction, both of which involves gelation/cross-linking at the same time. Hydrothermal reduction route is one of the easiest ways to make self-assembled graphene hydrogels (GHs) and this route employs high temperatures above 150 ^{o}C, and high pressure in autoclave.[40] The increased amount of hydrothermal reaction gives rise to further degree of reduction of GO, and this affects storage modulus, electrical conductivity, reported by Xu *et al.*[78] Chemical reduction route employs reducing agents such as vitamin C, hydrazine, hydroquinone, sodium ascorbate, ammonia boron trifluoride, or organic amines.[79] When oxygenated functional groups on GO sheets are removed, they are self-assembled into hydrogel by π-π interactions in acid or base condition.

Sol-gel synthesis is a common gelation-based route to obtain a monolithic graphene gel structure.[80,81] Gelation of the aqueous GO solution is carried out by reduction-induced self-assembly of GO nanosheets.[16,82] Reduction increases C/O atomic ratio and restores sp^2 nature of graphene sheets.[40,78] The hydrophobic interaction among rGO nanosheets causes phase separation which brings about gelation. These hydrogel structures are held together through physical (π-π stacking) and covalent crosslinks. These bonds are responsible for the electrical conductivity of these gels.

Our approach to synthesize GO hydrogels (Figure 8) involves sol-gel self-assembly of GO nanosheets with ammonium hydroxide followed by chemical reduction using sodium ascorbate. Ammonium hydroxide participates in covalent bond formation, improving the stiffness of GO hydrogels. Ammonia also helps in making the hydrogels more compressible. This compressibility of gels is crucial feature for structural energy storage applications, which is discussed in Section 5.

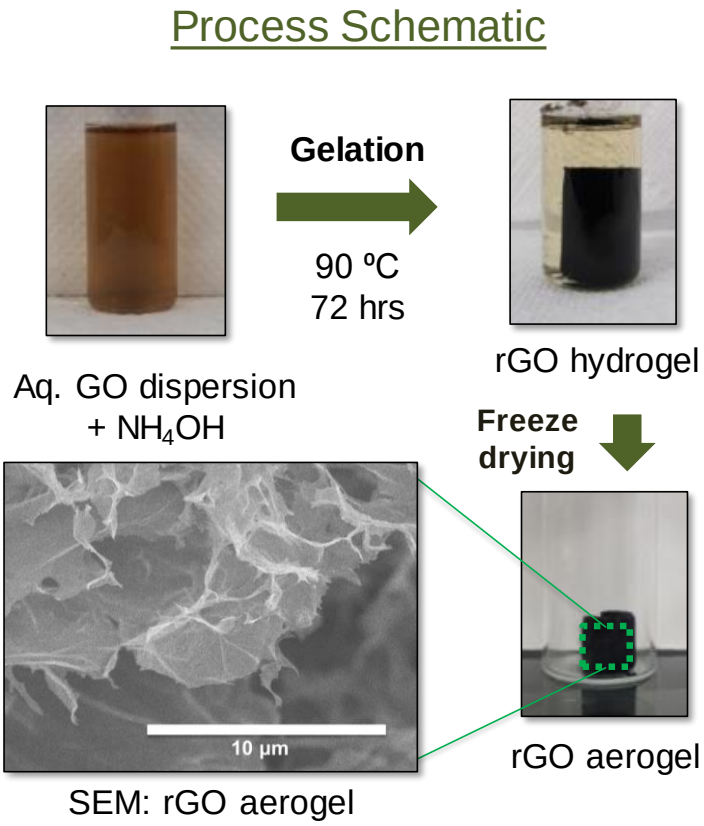

Figure 8: Schematic of sol-gel rGO gels synthesis. Gelation occurs from aqueous GO dispersion to obtain rGO hydrogel. SEM image shows microstructure of freeze dried rGO aerogel. Images provided by Shah, S.

3.2.2. Preparation of graphene aerogels

Production of graphene aerogel uses graphene hydrogel precursors, followed by freeze drying or supercritical drying. During drying process, solvents are replaced with gas phase material making porous structure and lighter structure. As a result, graphene aerogels exhibit high pore volume (2~3 cm^3 g^{-1}),[83,84] porosity (90~99 %), low density (0.012~0.098 g cm^{-3}), and low thermal conductivity (0.014 W m^{-1} K^{-1} at room temperature).[85]

Figure 9 shows multiple paths of drying; freeze drying, critical point drying and evaporative drying. Instead of evaporative drying, freeze drying and critical point drying is employed to maintain porous texture of precursor framework. This is because direct drying process leads to pore shrinkage, owing to capillary effects of surface tension of the solvent which cause pore collapse.[86] Freeze-drying goes through two phase transitions around triple point boundary of water. Firstly, temperature is lowered to get to solid phase and then pressure is reduced to make phase transition. This technique enables restricting capillary force attributed to water sublimation from solid to gas under vacuum.[55] Supercritical drying replaces the solvent with critical state fluid with low surface tension involved. For example, by using supercritical carbon dioxide, drying process is performed in low temperature as critical point of carbon dioxide is low (31.1 ºC at 7.39 MPa). Since high temperature and high pressure is not involved, surface tension is relatively less involved.

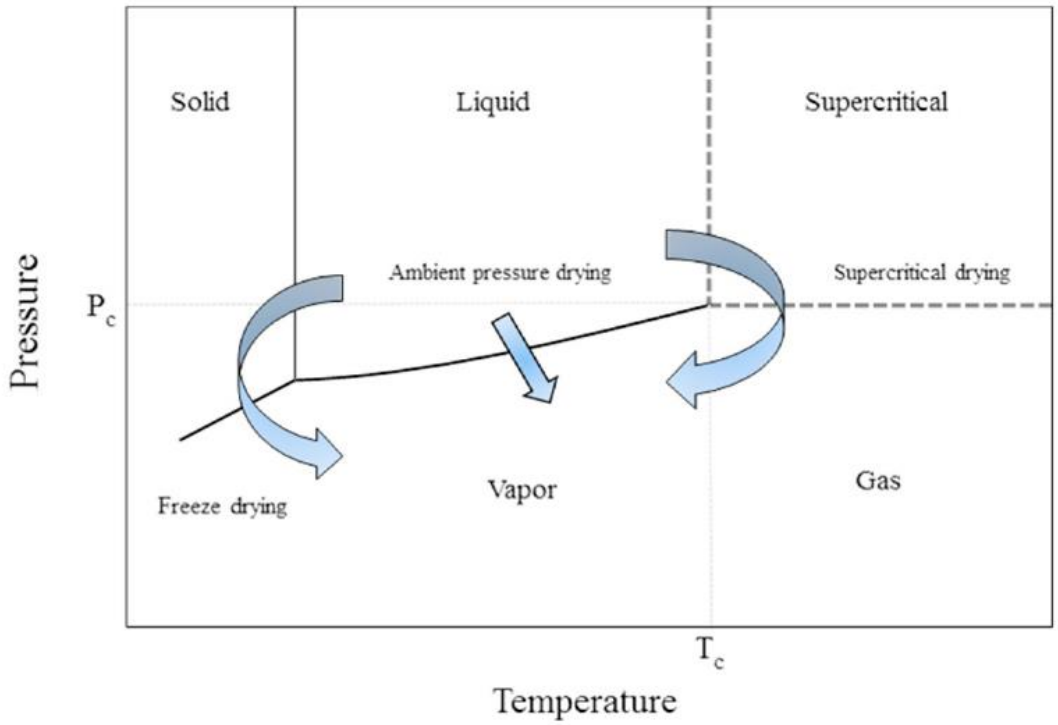

Figure 9: Phase diagram of water illustrating different drying routes as a function of pressure (vertical axis) and temperature (horizontal axis). Freeze drying goes through two phase transitions from liquid, solid and vapor in sequence to prevent structure collapse due to capillary forces. Supercritical point drying goes beyond the critical point. Reprinted with permission from ref.[14]

4. PERFORMANCE METRICS FOR STRUCTURAL ELECTRODES

4.1. Background of characterization technique

4.1.1. Characterizing mechanical properties of hydrogel (wet)

In this section, several mechanical characterization techniques for testing hydrogels are presented. Mechanical properties are classified in terms of deformation type (tensile, compressive and shear) or deformation mode (dynamic/oscillatory or static). Typically instruments like nanoindentor, dynamic mechanical analyzer (DMA), rheometer and universal test-frame are used for measuring mechanical properties (Figure 10).

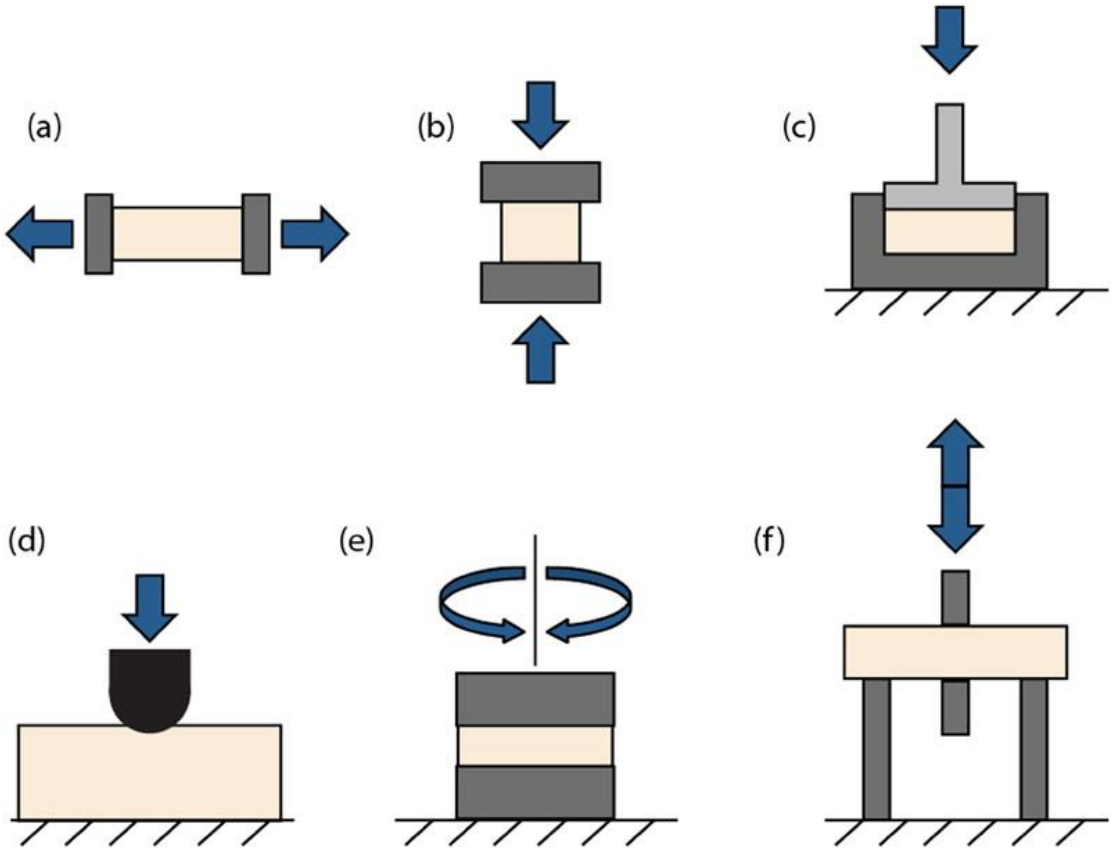

Figure 10: Schematic of mechanical testing methods of hydrogels: (a) tension (b) compression (c) confined compression (d) indentation (e) shear rheometry (f) bending modes of dynamic mechanical analysis (DMA) test. Applied force is indicated by blue arrow. Skin color indicates samples. Black color indicates testing device. Reprinted with permission from ref.[7]

Through static tensile tests, Young's modulus, a measure of stiffness, and ultimate strength is obtained from load and displacement data. In static compression tests, uniaxial compression load is applied between two parallel plates. The stress and strain data can be used to calculate compression modulus and determine elastic compression regime. Static

shear tests give information about shear modulus and shear yield stress. These static tests can be conducted either in universal test-frame or DMA. However, DMA is also useful for conducting dynamic tensile and compression tests. This approach can be used to determine tensile storage and loss modulus (E' and E") which are representative of elastic and inelastic behaviors of the gels.

For tensile tests in DMA and universal test-frame, gripping sample is an important issue when testing hydrogel.[7] To solve this issue, cardboard tabs, double sided tape and glue is used to grip the sample[87]. Compression test can be performed in two different ways; one is confined test and the other is unconfined test.[88] In unconfined test, sample is placed between two non-porous platens and compressed[89]. In confined test, sample is confined in a container and compressed by a single porous plate. The latter test is more suitable for hydrogel samples because fluid in hydrogels can be squeezed out through a single porous plate. [90]

In oscillatory rheology test (Figure 11), a sample is placed between two plates and plates deform the sample with certain shear rate and shear strain.[1] Storage modulus (G') indicates sample's elastic behavior, which refers to how much energy can be stored during deformation in an elastic manner. G' is related to the extent of cross-linking, while. G'' indicates energy dissipated during loading cycle.[91]

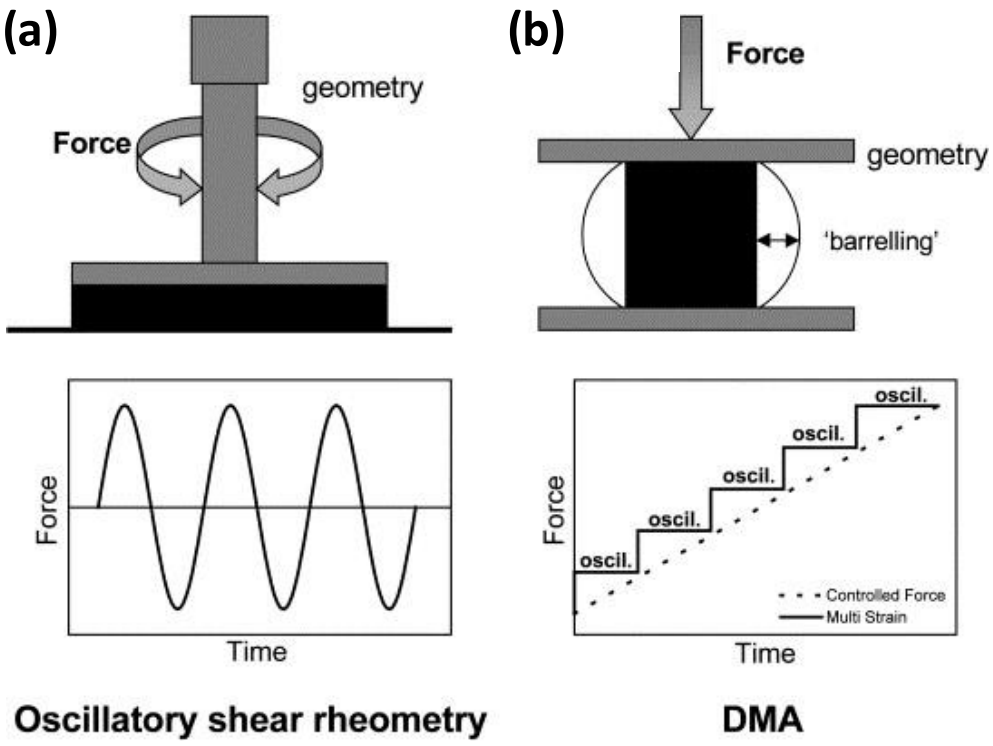

Figure 11: A comparison between the use of dynamic mechanical analysis (DMA) and oscillatory shear rheometry for mechanical characterization of hydrogels. Illustration of (a) oscillatory shear rheometry, and (b) DMA. The graphs below each testing illustration show applied force as a function of time; in oscillation mode, shear forces are applied under constant strain. DMA mode is multi-strain mode that applies a series of increasing oscillatory compressive forces. Reprinted with permission from ref.[1,2] (Meyvis, 2002)

Tensile or compressional storage modulus obtained from DMA and shear storage modulus calculated from rheometer are not same since they result from different kinds of deformations; they can be related by the equation below.

$$E' = 2G'(1 + \mu) \quad (2)$$

μ is Poisson number (the number for ideal elastic rubber is 0.5).[92]

Rheometer is particularly used for analyzing gelation process because it is capable of testing viscoelastic liquids and solids. Under constant shear amplitude and frequency, it can measure the change in G' and G'' with time.

Our group utilizes rheometer to evaluate the storage modulus and yield strain of the GO hydrogels. One of the challenges we faced is slipping of hydrogel on the surface of parallel plates at high shear amplitudes. In such scenario, the shear properties measures will be representative of the interface between the gel and the plates, and not the sample itself. In order to prevent slipping, we modified the parallel plate surface with sand paper or used parallel plates with crosshatched surface. These profiled surfaces will increase the tackiness between gels and plates enabling us to measure the yield strain to evaluate the shear mechanical properties of GO hydrogels.

4.1.2. Characterizing mechanical properties of powder (dry)

Powder-based materials exist incorporated into composite. To test powder materials, adhesion and cohesion indicate mechanical performance. Adhesion is an attractive force between different components, while cohesion strength refers to intermolecular attraction. Peel test measures adhesion or tensile strength (Figure 12).[11] On current collector, powder

materials should be attached and tape is required in a form that one side of it is fixed and the other side is the free end. Then, the test measures the force required to peel the tape. If adhesion strength of the electrode to the current collector is bigger than cohesion strength, part of the electrode would be removed from the current collector.[6,93,94] The opposite outcome tells that adhesion and cohesion strength of the electrode to the foil is bigger than adhesion of the tape to the electrode, so most of the electrode will stay on the foil.

Drag test is suitable for measuring thin film structures.[95] It measures horizontal forces as the tip is dragged through the electrode; the tip should be wider than the average particle size in the electrode so that it removes the electrode material on the foil. The measured force depends on conductive additives.[96]

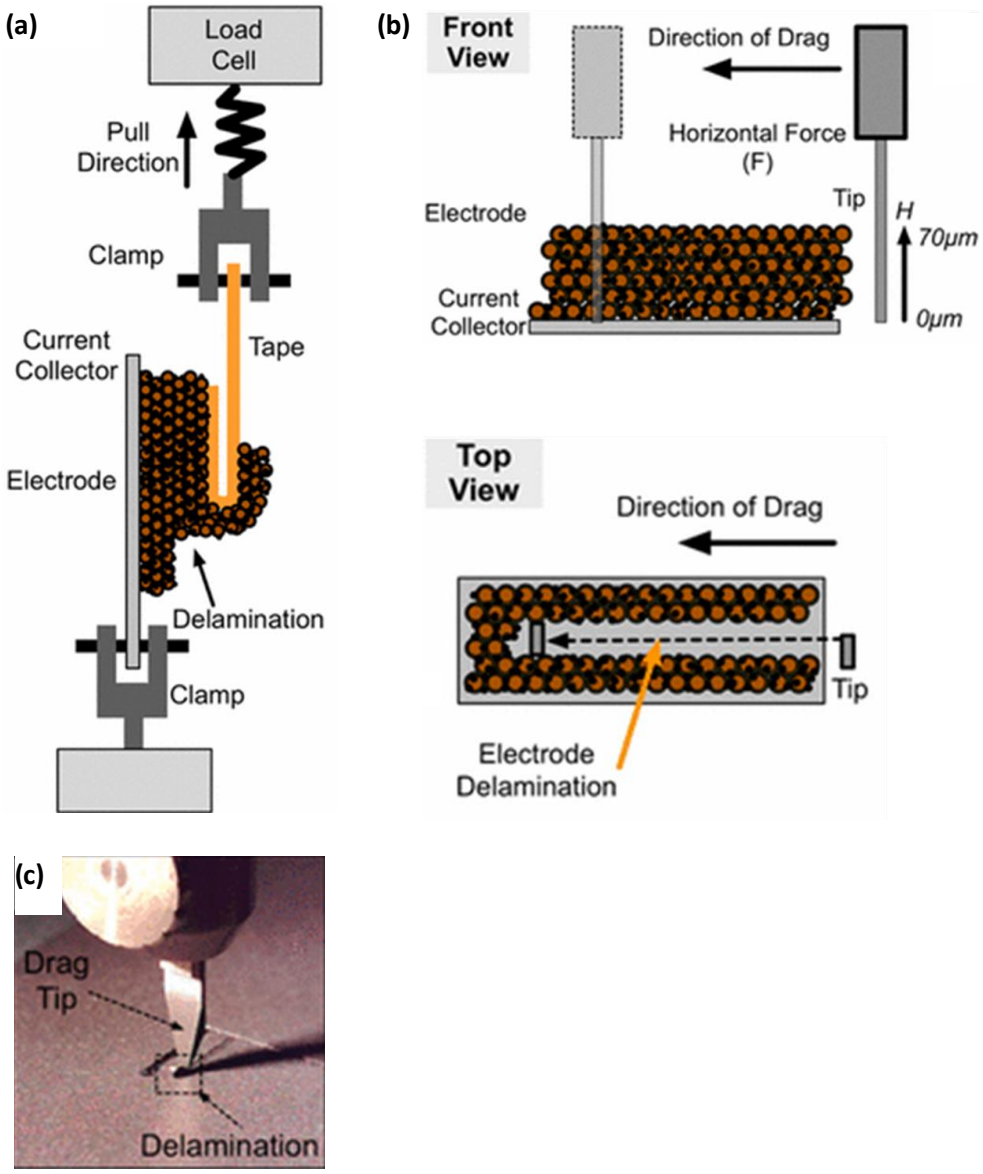

Figure 12: Schematic of peel test, and drag test (a) Peel test: force applied on the tape is measured while delamination occurs in the electrode materials (b, c) Drag test: force applied on drag tip is measured when delamination occurs. Reprinted with permission from ref.[11]

Bending tests are widely employed technique to evaluate the strain tolerance[6]. By calculating the actual strain from bending radius 'r' (Figure 13), strain tolerance of the materials is assessed. Subjected to bending, materials go through two different mechanical deformation; tension and compression and there are three major experiments that can be performed: 1) before and after measurement under a single bending, 2) cyclic measurements 3) specific performance metrics during bending deformations.

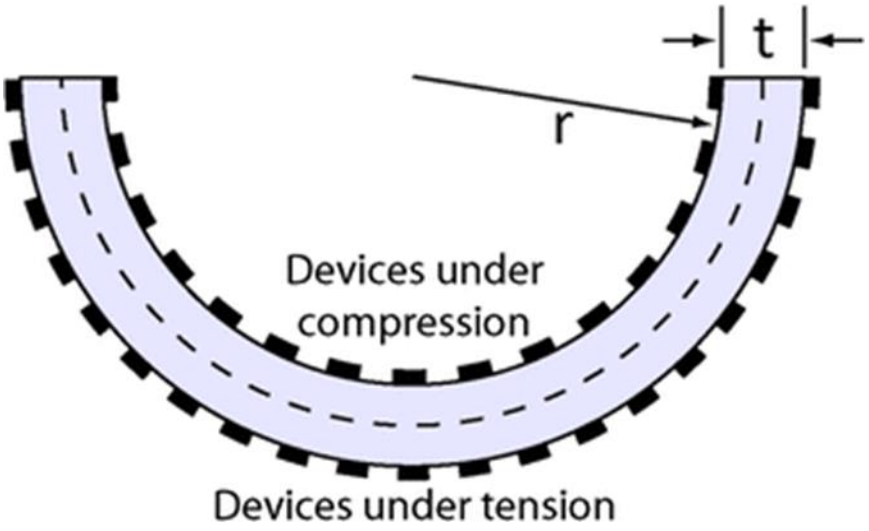

Figure 13: Conceptual drawing of bending deformation involving compressive and tensile strains. Black dashed line represents mechanically neutral plane. 'r is bending radius, and 't' is thickness. Reprinted with permission from ref.[6]

4.1.3. Electrochemical properties

As explained in Section 1.3, energy storage mechanisms in supercapacitors emerge from reaction at electrode/electrolyte surface. The reaction occurred in EDLC involves electrostatic charge separation and accumulation/ When calculating capacitance of supercapacitors, one can use cyclic voltammetry (CV) or galvanostatic charge/discharge cycling.

Cyclic voltammetry (CV) is a technique for quantitatively analyzing reactions. To generate function, potential is applied between E_1 and E_2 during a single cycle in a triangular waveform as indicated in Figure 14 (b). CV profile (Figure 14 (d)) tells reversibility of the reaction, and whether it is kinetically limited or diffusion limited. For batteries, CV basically analyzes characteristic parameters, such as anodic peak current, cathodic peak current, anodic peak potential, and cathodic peak potential. By changing with scan rate, these parameters are adjusted. For supercapacitors, CV profile shows resultant current from applied potential. Figure 14 (d) shows CV profile of a symmetric carbon double layer supercapacitor. Device capacitance is expressed as :

$$C_{device} = \frac{\int_{v1}^{vn} idV}{v \times \Delta E} \quad (3)$$

v is scan rate (V/s), ΔE is voltage window (V), i is a measured current at the applied voltage V, which can be calculated from CV.

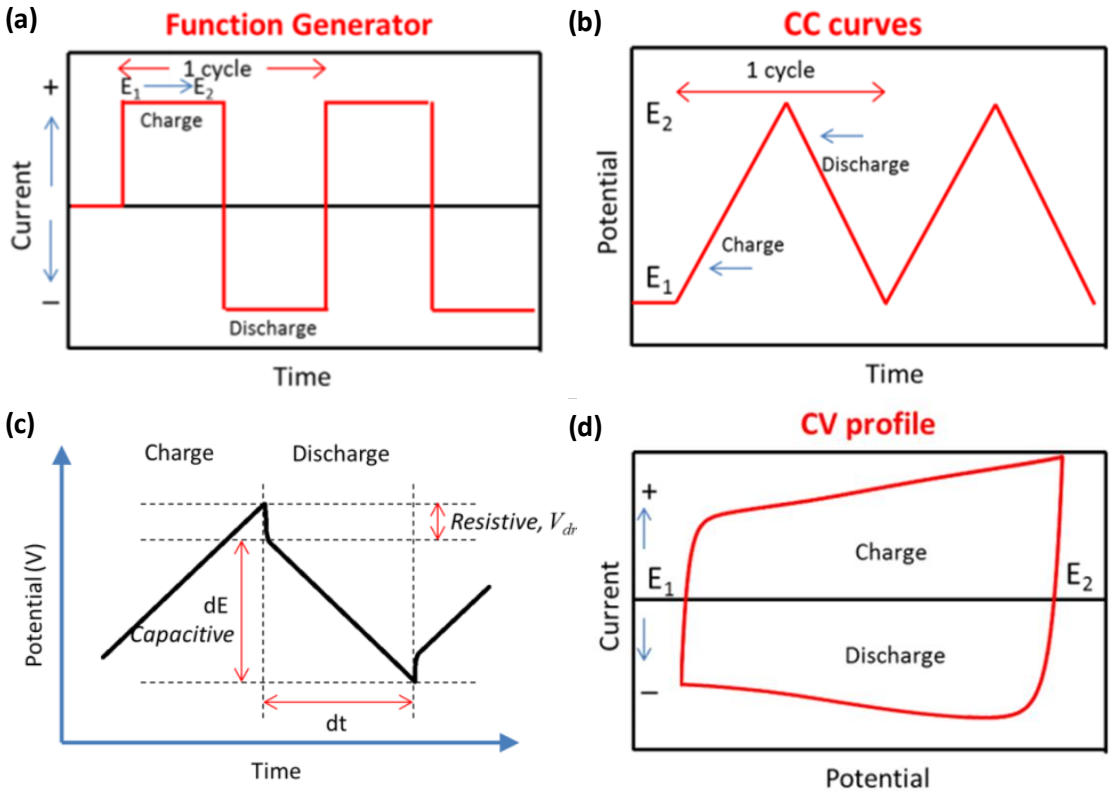

Figure 14: (a, b, c) Galvanostatic charge/discharge curves (CC) and (d) CV curve of supercapacitors. (a) step current change as input (b) linear potential change as output during charge and discharge (c) constant current charge/discharge profile (d) CV profile of a symmetric carbon EDLC. Reprinted with permission from ref.[4] (El-Kady, 2013)

Galvanostatic charge/discharge cycling (CC) is a constant current measurement. As an input, step changes of current are applied (Figure14, a), so output potential changes (Figure14, b). It is more reliable than other techniques because it represents the real world operation where charge and discharge occurs at constant current. Figure14 (c) shows galvanostatic charge/discharge profile for supercapacitor.[4] *dE* is the voltage change during

discharge (V), *dt* is discharge time (s), *V* is voltage drop caused by equivalent series resistance (ESR). Capacitance of the device is calculated as below,

$$i_{app} = V_{drop} \times ESR \tag{4}$$

$$C_{device} = \frac{i_{app}}{-dE/dt} \tag{5}$$

i_{app} is discharge current, and $-dE/dt$ is discharge curve slope.

Specific capacitance of electrode are calculated from device capacitance:

$$C_{s,device} = \frac{C_{device}}{M} \tag{6}$$

$$C_{s,electrode} = 4 \times C_{s,device} \tag{7}$$

M is the mass of active material in the device.

Volumetric capacitance of the device and electrode are calculated in the same way.

$$C_{v,device} = \frac{C_{device}}{V} \tag{8}$$

$$C_{v,electrode} = 4 \times C_{v,device} \tag{9}$$

From galvanostatic charge/discharge curves, energy is calculated as follows,

$$Energy = It\frac{\int Vdt}{\int dt} \quad (10)$$

I is the discharge current, *t* is time passed between cutoff voltages, *I*t = Q* which is the charge passed. *V* is voltage; in this equation, average voltage is calculated.

Coin cell is for characterization of electrochemical performance. GO gel/H_2SO_4/GO gel symmetric coin cell is illustrated in Figure 15, there are several components in cell assembly. Stainless steel cylinders are used to keep all the components contacted to prevent failure. Platinum foils work as current collector. For active materials, GO gels are free-standing electrode with thickness 100 μm. Between two electrodes, Celgard film is

the separator. Testing through coin cell, electrochemical performance is calculated from CV response and resistance.

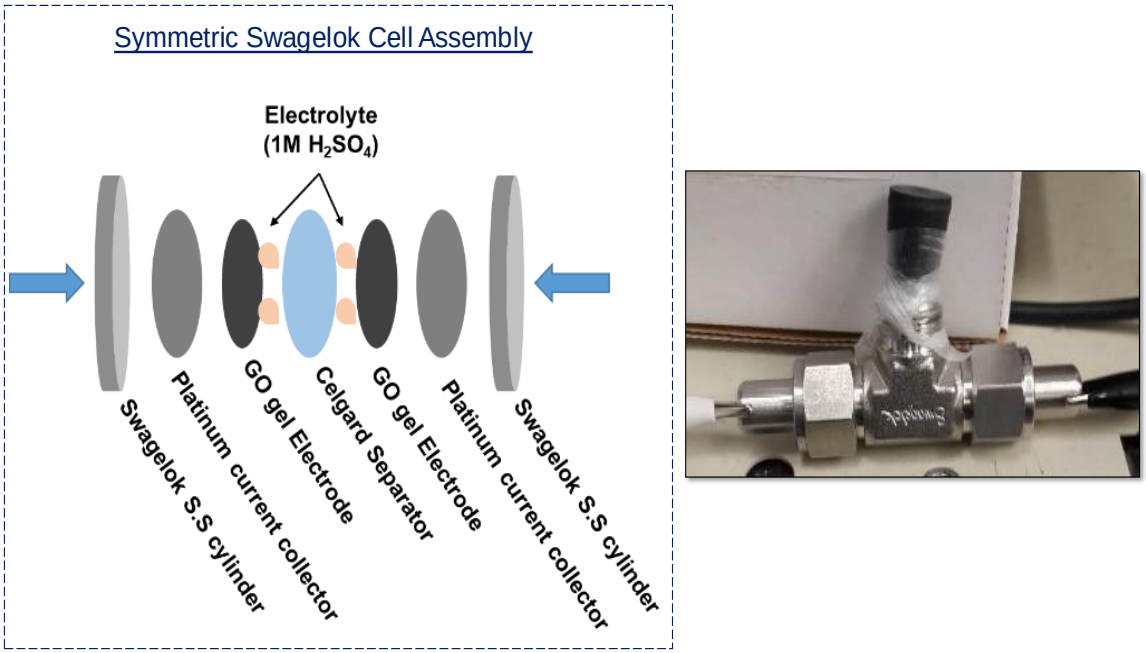

Figure 15: GO gel/H_2SO_4/GO gel symmetric coin cell used for supercapacitor device testing. Platinum foils act as current collectors. Free-standing GO gels are electrodes. Celgard film is used as a separator between two electrodes. Images provided by Shah Smit and Kwon SeRa.

5. OUR EXPERIMENT AND RESULTS SO FAR

Our sol-gel synthesis method for GO hydrogel is presented in Section 3.2.1. To improve the mechanical properties of GO hydrogels, we considered adding aramid nanofibers (ANFs) in GO hydrogels. ANFs are a nanoscale version of Kevlar. ANFs are formed by reacting commercial Kevlar K69 thread with a polar aprotic solvent (like DMSO) and inorganic base (like KOH). Typically, ANFs are obtained as colloidal dispersion in a solution of DMSO saturated with KOH. Addition of proton donating solvents like water/ethanol results in coagulation of ANFs due to protonation of surface amide groups, causing loss of surface electrostatic repulsion.

GO-ANF hydrogel composites with homogeneously distributed ANFs are obtained by using a combination of solvent exchange approach and sol-gel gelation method. A dispersion of GO in DMSO is obtained by solvent transferring GO from water to DMSO using a rotary evaporator. Miscibility of DMSO with water and high boiling point of DMSO is crucial for this approach. GO in DMSO dispersion is mixed with ANF in KOH-saturated DMSO dispersion using magnetic stirring and bath sonication. Water is added to this solution while stirring to induce hydrogen bonding between GO and ANFs. This homogeneous slurry of GO and ANF in DMSO is washed with water through dialysis for gelation, as sol-gel approach is limited to aqueous systems.

For mechanical characterization of GO/ANF hydrogels, we carried out rheology test by employing oscillatory amplitude sweep with shear frequency of 1 rad/s. We tested GO only hydrogels first, then GO with different ANF content were tested. For rheology testing, GO hydrogel was sliced and placed between parallel plate geometry equipped with crosshatched surface to prevent slipping (Figure 16, a). Storage modulus (G') of GO hydrogel was 469 kPa indicated by red color (Figure 16, b). Loss modulus (G'') values are one order of magnitude lower than the G' indicated by green color. G' starts to decrease because shear stress becomes constant with respect to increasing shear strain.

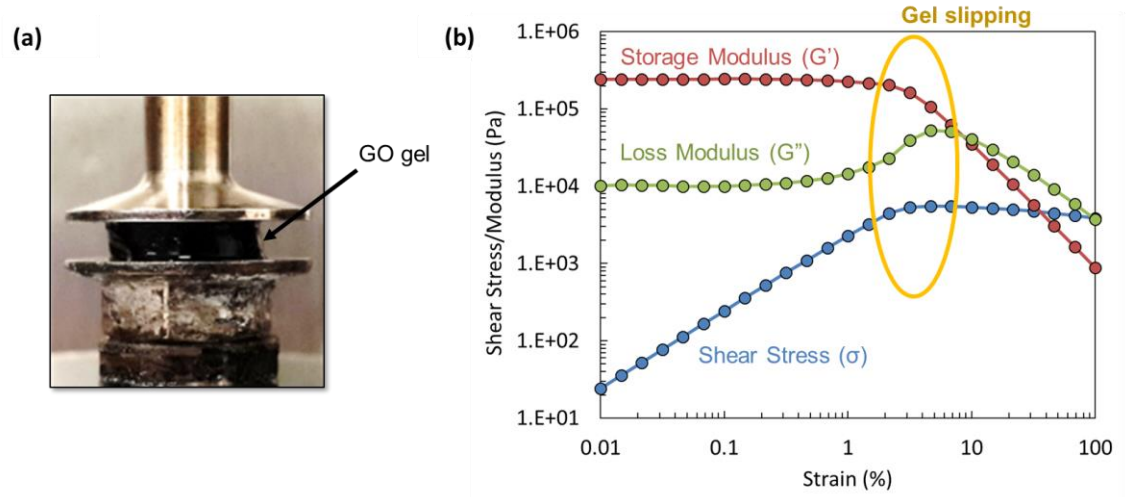

Figure 16: Rheology test for mechanical characterization of GO/ANF hydrogels. (a) Oscillatory rheology on GO hydrogel slices to obtain storage modulus and yield strain. Hydrogel sample is placed between two plates and oscillatory force is applied. (b) Graph showing storage modulus (G'), loss modulus (G''), and shear stress. Images provided by Shah, S.

In figure 17, G' for 1, 2, 5, 10, 15% ANF content GO gel are indicated. With increasing content of ANF from 2%, G' of GO/ANF hydrogels decreases. This indicates that although ANFs may act as reinforcements in GO structures, they also disrupt the gelation process.

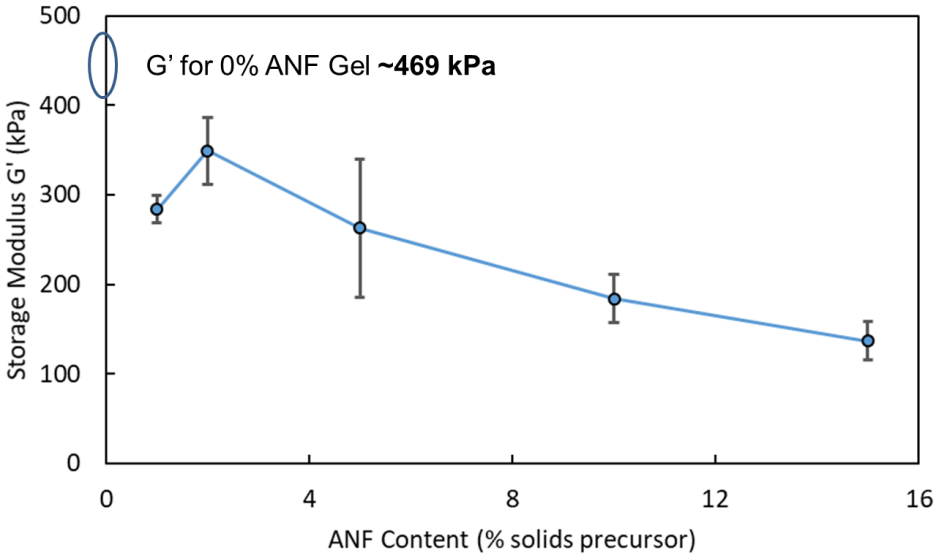

Figure 17: Mechanical Properties of GO-ANF gels with different ANF content (1, 2, 5, 10, 15%). Maximum G' value reaches 469 kPa without ANF content. Images provided by Shah, S.

6. SUMMARIES OF LITERATURE REVIEW AND COMPARISON: ASSESSING PROPERTIES OF MULTIFUNCTIONAL ELECTRODE MATERIALS

When it comes to assessing properties of multifunctional electrode materials, it is notable to understand which metric should be used to evaluate electrochemical and mechanical properties of the materials. As introduced in Section 2.3, specific capacitance and conductivity are the commonly investigated metrics for electrochemical performance; for mechanical performance, stiffness, strength and toughness are evaluated. In this section, graphene-based architectures and their advantages and disadvantages are discussed. These include gel-, paper-, and powder- based electrodes among which gel materials are more discussed. Furthermore, this work includes on GH electrodes and comparison of it against other non-gel electrode materials as well as aerogels.

There are several issues that should be considered for assessing and comparing electrode materials for supercapacitors. When comparing monolithic graphene gels against traditional powder-based and paper-based graphene electrodes, one needs to consider the fact that a practical device requires a considerable amount of electrode material. In some studies, specific capacitance obtained from a working electrode containing only a small amount of active materials is reported.[75] However, performance is not linearly related to the amount of material. Additionally, the weight of current collector, electrolyte, and separator has an impact on energy storage device. It was suggested by Gogotsi *et al*. that there is no standard in reporting a device performance for

thin film electrodes. Practical electrode thickness is 100~200 μm. However, in some studies, the electrodes are 10 times thinner and they show much higher capacity and conductivity. This also makes it problematic to extrapolate the data for comparison, so caution should be exercised in comparing the results of one study against another.[97]

For a comparison of gel monolith electrode with traditional powder electrode as crushed version of the monolithic architecture, Wen *et al.* synthesized nitrogen/phosphorus co-doped graphene monolith (N/P-GM) and measured its electrochemical properties.[17] N/P-GM is cut into 5 mm thickness and pressed into a film (Figure 18: a, b). The powder electrode was created by mixing grinded powder of N/P-GM, 5% carbon black, and 5% polyvinylidene fluoride (PVDF); the resulting electrode was named N/P-GP (Figure 18: c, d). They reported lower charge transfer resistance and higher specific capacitance (213 F/g at 0.05 A/g) of N/P-GM compared to the prepared N/P-GP (183 F g^{-1}), however, along with increasing current density, N/P-GM have poor rate capability showing lower capacitance at higher current density (Figure 22: e, g, f). In

figure 18 (f), drastic iR drop was observed on N/P-GM at 1 A/g, compared to its triangular shape at 50 mA/g (Figure 18, e).

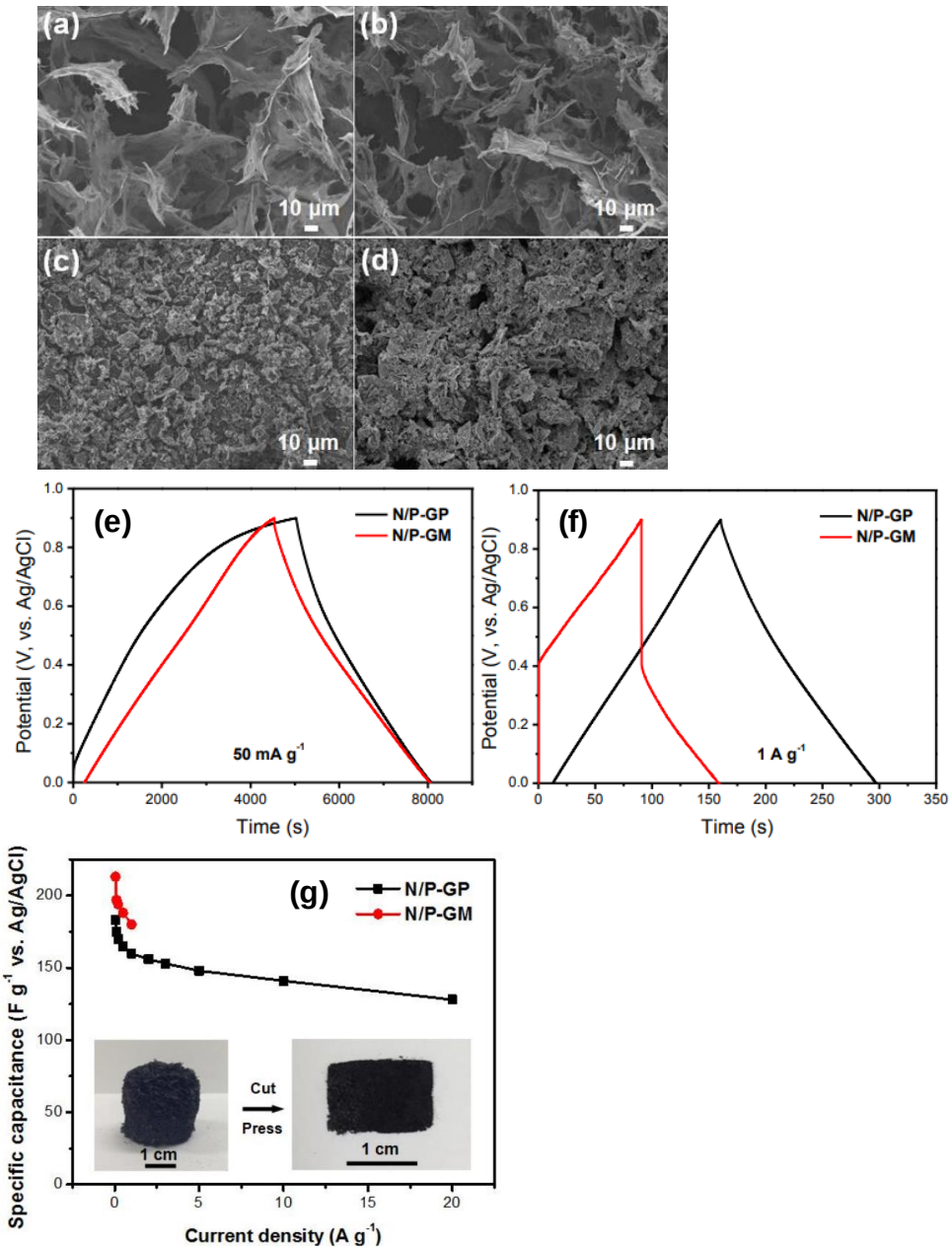

Figure 18: Comparison of electrochemical properties of nitrogen/phosphorus co-doped graphene monolith and conventional powder electrode. (a) as-prepared N/P-G monolith, (b) pressed N/P-G monolith, (c) N/P-G grinded powder using mortar, (d) conventional electrode (N/P-GP). (e, f) cyclic voltammetry of N/P-GP and N/P-GM at 50 mA/g and 1 A/g, respectively. (g) the specific capacitance of N/P-GM and N/P-GP in 1M H_2SO_4 electrolyte in three-electrode cells. Reprinted with permission from ref.[17] (Wen, 2016)

Paper-like graphene electrode (vacuum-filtration technique): Graphene papers are typically prepared by vacuum filtration and favorable for thin and portable electronics. Vacuum filtration (another name for flow-induced method) employs a pressure gradient that allows variable filtration rate.[98] This technique is not only used for producing graphene papers, but also used to add another component like spheres, particles, and fibers between graphene sheets. To obtain graphene papers, liquid solution in GO suspension is filtered out through membrane filter with directional flow. Consequently, all left is graphene. The obtained graphene paper can be monolayer or multilayers thickness, which is controllable.

Generally, paper-like graphene electrodes are useful for applications where high stiffness and strength are representative features. Young's modulus and yield stress are significantly higher for paper-like graphene than gel-based electrodes. However, they suffer from low strain-to-failure. Moreover, their compact structure damages capacitance performance since they have low specific surface area that hinders rapid electrolyte diffusion. When paper-like graphene electrode is subjected to mechanical deformation, its mechanical integrity as well as electrochemical functions can be easily lost.

To investigate mechanical behaviors of dense and aligned graphene architecture, Ruoff's group carried out filtration of chemically exfoliated graphene, yielding layered GO paper.[18] The resulting GO paper has high Young's modulus (~32 GPa), fracture strength (~130 MPa), and toughness (350 kJ m^{-3}). However, the ultimate tensile strain for

GO paper was low as 0.6%. They also suggested that under bending and uniaxial tension, GO paper shows more flexibility onto bending, which is depicted in Figure 19. More deformation is sustained during bending than tensile stress due to its aligned layered structure. Tensile load are applied homogeneously while bending induces concentrated stress on the GO paper surfaces.

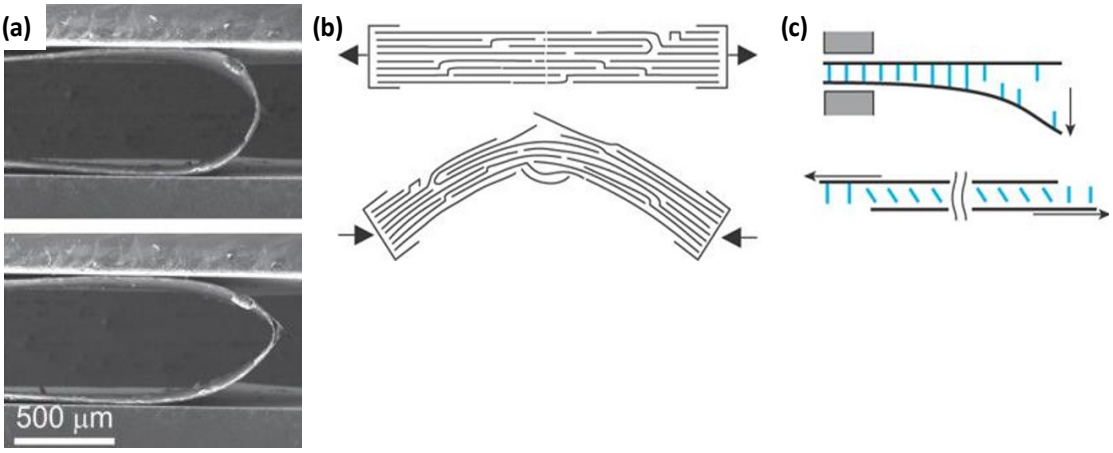

Figure 19: Schematic illustration depicting different mechanical behaviors of GO paper on bending test and tensile test. (a) SEM images of GO paper for bending test. The sample (5.2 μm thickness) is placed between two parallel plates and compressed until kink is formed (below). (b) Schematic of bending test. Delamination occurs along voids within layered structure. (c) Schematic of bending test and uniaxial in-plane tensile test. Blue color represents water molecules binding adjacent GO sheets together. These interactions are degraded upon bending, and upon applied tensile load. Reprinted with permission from ref.[18]

One of the notable factors on capacitance performance is that the material was tested on either wet state or dry state (Figure 20). For example, Li *et al.* produced rGO wet film and compared it to freeze-dried film.[19] Starting with GO solution, ammonia and hydrazine were added to it to induce reduction (90 ºC for 1 hour), followed by vacuum filtration.

Consequently, self-stacked, solvated graphene (SSG) film was obtained (Figure 20: a, b, c, d). Specific capacitance measured from this wet rGO film exhibited 215 F /g as a maximum value, and 72.8 % of it was retained under high current density (1080 A/g) shown in (Figure 20, g). For comparison, freeze-dried samples exhibited poorer capacitance performance (25 F/g at 200 A/g). The reason for superior capacitance performance of SSG film is that water as spacers ensures interlayer space to prevent restacking of rGO sheets. SSG film displays highly open, porous, ordered and well-interconnected structure than dried film. Through drying step, significant restaking, and volume shrinkage causes decrease in surface area and pore volume that are key factors for ion diffusion. Accordingly, capacitance performance is restricted.

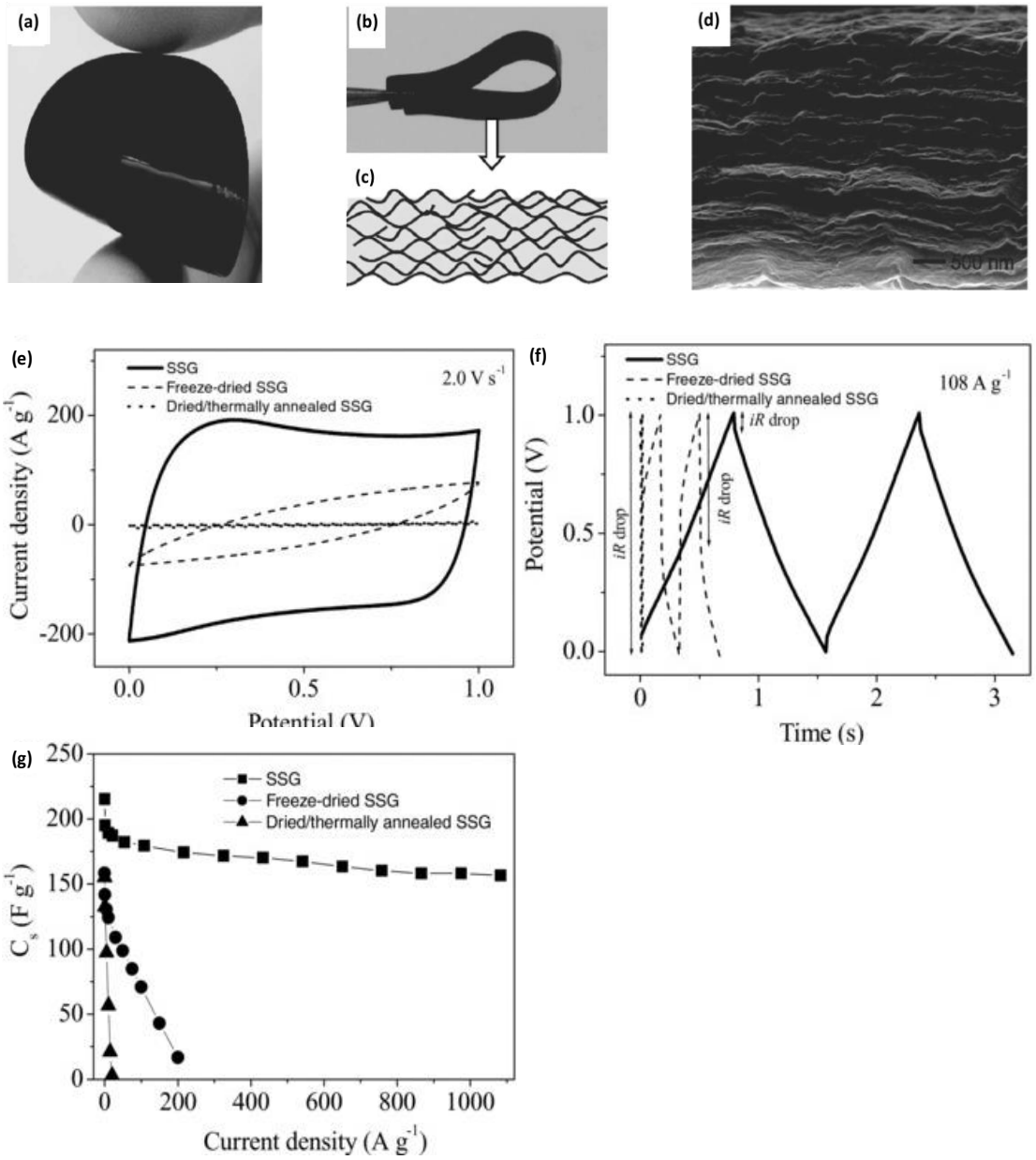

Figure 20: Electrochemical performances of rGO films (a, b) images showing flexibility of the wet rGO films. (c) cross-sectional image of the wet rGO films. (d) SEM image showing of freeze-dried rGO film. (e) CV curves at fast scan rate 2 V s^{-1}. (f) Galvanostatic charge/discharge plots at current density 108 A g^{-1}. (g) Plot showing specific capacitance (y-axis) at varying current density (x-axis). All the tests were carried out in 1M aqueous H_2SO_4 electrolyte. Reprinted with permission from ref.[19]

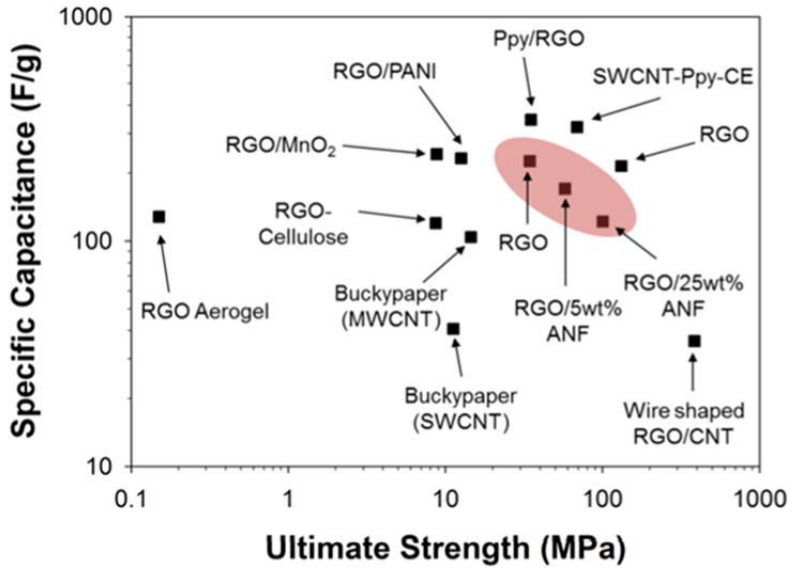

Figure 21. Ashby plot showing comparison of rGO/ANF composite against free-standing paper electrodes. Reprinted with permission from ref.[9] (Kwon, S. R.; Harris, J.; Zhou, T.; Loufakis, D.; Boyd, J. G.; Lutkenhaus, J. L. Mechanically Strong Graphene/Aramid Nanofiber Composite Electrodes for Structural Energy and Power. ACS Nano 2017, 11, 6682-6690.). Copyright (2017) American Chemical Society.

Kwon *et al.* prepared vacuum filtered rGO/ANF paper electrode and achieved good combination of electrochemical properties and mechanical properties.[9] With addition of ANFs, rGO-ANF paper electrodes displayed enhanced stiffness, strength, and toughness. The obtained 25% ANF/rGO showed higher Young's modulus (13.0 GPa), tensile strength (100.6 MPa) and toughness (427.4 kJ/m^3), compared with prepared rGO paper; Young's modulus (3.7 GPa), strength (34.4 MPa), and toughness (182.3 kJ/m^3). They reported that oriented graphene layers and ANFs played a critical role in improvement of mechanical properties. This improvement is attributed to hydrogen bonding and π- π interaction between graphene sheets and ANFs. However, capacitance values decrease when ANF

contents increase. At current density 0.5 A/g, 25 wt% ANF/rGO showed lower specific capacitance (88 F/g) than rGO paper (215 F/g). To see how these trade-offs are competitive against other free-standing paper electrodes, they plotted ultimate strength versus specific capacitance (Figure 21). As a result, rGO/ANF paper exhibited good combination of both properties than other rGO-based and CNT-based paper materials.

Gel-based electrodes: Graphene-based gels are 3D monolithic structures with high porosity. Electrochemical properties of graphene gel-based electrodes are emphasized in literature works whereas mechanical properties are rather less studied. They have high specific capacitance since their 3D open interconnected porous structure renders accessible surface area. Unlike paper-like electrodes, mechanical properties of gel-based electrodes are not much attractive in terms of stiffness and strength because of its elastic behavior. Typically, their strengths are in the order of kPa whereas paper-like electrodes are in the order of MPa or GPa. Commonly measured mechanical properties of gel monoliths are compressibility with loading and stability under cycles. It is suggested that graphene gels are favorable for their outstanding compressibility without fracture, which refers to high yield strain and recoverbility.[99] For instance, rGO aerogels recover its original shape even after it was compressed with 80% strain, and they support more than 14000 times their own weight.[83,100,101] Thus, gel-based electrodes are advantageous when mechanical compressibility plays an important role for application like deformation-tolerant power sources and electronic devices and when used in the wet state with aqueous electrolyte.

For their ability to manage energy and power, their porous architecture renders a high surface-area to-volume ratio. This feature enables improved energy availability with one time of charging than activated carbon. Additionally, power performance of monolithic structure stands out when compared with compact structure. However, reduction step have an influence on this feature. Since reduction of GO sheets leads to hydrophobic behavior which is not preferred for ion-accessibility, rGO sheets show reduced specific capacitance. To preserve capacitance value with reduction step, several studies use a functionalization method of graphene sheets that employs doping (nitrogen, boron, sulfur, and phosphorus),[102-104] or modifying with compounds (hydroquinone, 1-pyrenecarboxylic acid, 2-aminoanthraquinone, and benzoxazole).[105-107] Accordingly, chemical properties are enhanced and aggregation of graphene sheets can be prevented at the same time, resulting in improved capacitance performance.[108] For instance, Yu *et al.* showed nitrogen-doped graphene hydrogel having ultrafast charge/discharge rate (at a current density of 185 A/g) with a high power density of 205.0 kW/kg and moderate energy density[109]. The nitrogen doping facilitates charge transfer between carbon atoms causing the electrochemical performance enhancement. The material exhibits a specific capacitance of 113.8 F/g and 95.2% of its capacitance is retained at a high current 100.0 A/g over 4000 cycles.

Wet gel vs dry gel: Hydrogels and aerogels are distinguishable by their wet or dry state. Our rationale for keeping gel wet was inspired by the fact that in real application, electrodes are more or less wet. In contrast, most of materials are reported in a dried form

even though their final uses involve the contact with a liquid such as in supercapacitors. When comparing GHs and GAs, what makes it difficult to compare electrochemical performance is that aerogels are characterized in wet state with electrolyte. Since aerogels (dry gel) are produced from hydrogel precursors (wet gel), their re-wetting issue is notable in that it involves additional complexity and cost to the process. As a result, GH makes full use of high surface area offering active sites for charging, as well as prevents graphene agglomeration, which can explain the higher specific capacitance of GH than re-wetted GA.[110] Moreover, the liquid-filled GH offers highly efficient ion transport channels in aqueous electrolyte due to existence of water. Ma *et al*. compared capacitance GH with GA and found that GH (43.61 F g^{-1}) had more than two times higher capacitance than GA (18.65 F g^{-1}).[110]

Sheng *et al*. self-assembled GH made from aqueous GO dispersion (GO 2 mg mL^{-1}) followed by chemical reduction with sodium ascorbate. The GH exhibited high capacitance of 240 F g^{-1} calculated by galvanostatic charge/discharge tests at current density 1.2 A g^{-1} (Figure 22: a, b).[16] The sample was prepared as 2 mm sliced GH, and the electrochemical tests were carried out in three-electrode system in 1M aqueous H_2SO_4 electrolyte. For measuring mechanical performance, they performed dynamic frequency rheology test with oscillatory strain of 0.2% on 25 mm diameter parallel plate geometry at 25 ºC (Figure 22: c). G' of the prepared GH was 275 kPa at 10 rad /s.

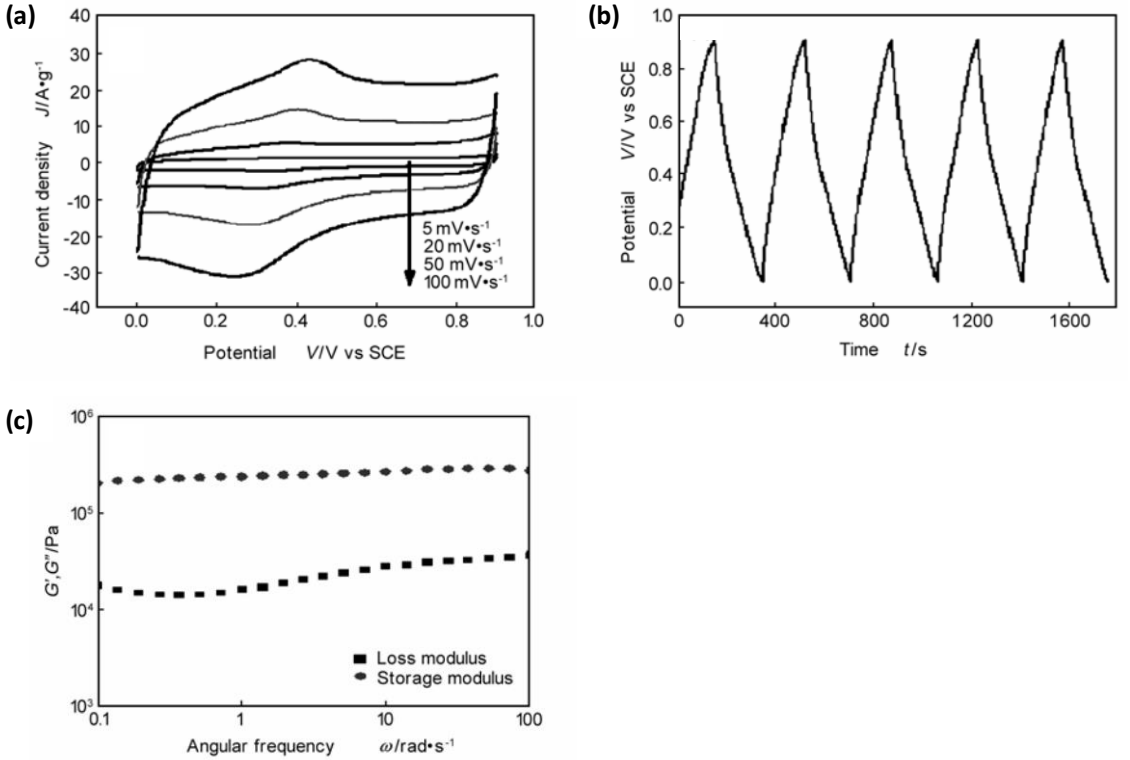

Figure 22: Electrochemical behavior and mechanical behavior of graphene hydrogels prepared by hydrothermal method. (a) CV profile of a GH electrode in 1.0 M H_2SO_4 at different scan rates. (b) Galvanostatic charge/discharge curves of the GH electrode at 1.2 A g^{-1} (c) rheological behavior of GH. G' values are one order of magnitude higher than the G''. Reprinted with permission from ref.[16]

It was studied by Xu *et al.* that reduction degree affects properties of GHs. To figure out this, they carried out rheology test and compression test for measuring mechanical properties of hydrothermally reduced GHs.[111] Depending on different reduction degree of GO, self-assembled GHs showed changes in conductivity, storage modulus, and compressive elastic modulus. With increasing hydrothermal reaction time (1 to 12 hours), further reduced samples revealed stronger mechanical behavior. Increase in storage modulus was observed from 55 to 470 kPa and compressive modulus increased from 29 to 290 kPa. Conductivity also increased with reduction degree, ranging from 0.23 to 4.9 mS/cm.

Several prior studies investigated pH dependent reduction and gelation. Hu *et al*. prepared four samples with different amount of ammonia during hydrothermal reduction.[8] With increasing amounts of ammonia (higher pH) from 60 (GHG-N-290) to 290 μL (GHG-N-290), the graphene hydrogels is subjected to volume expansion more than 70% from 0.86 cm^3 (no ammonia addition) to 1.48 cm^3 (highest ammonia addition). The resultant different porous structures are shown in Figure 23. Moreover, the observed changes on properties are conductivity drop by 15-40 %, 40% lower elastic modulus (370 kPa to 192 kPa), and 60% lower yield strength (33 kPa to 12 kPa) compared to hydrogel samples without ammonia (Table 1). These properties are attributed to thicker pore walls of no-ammonia hydrogels than ammonia added samples. Although no-ammonia rGO hydrogels exhibit stronger mechanical behaviors, they are more prone to failure on compression (lower strain-to-failure, 45%) than GHG-N-290 (around 60%).

Table 1: Electrical and mechanical properties of graphene hydrogels with different amount of ammonia addition. Reprinted with permission from ref. [8] (Hu, K.; Xie, X.; Szkopek, T.; Cerruti, M. Understanding Hydrothermally Reduced Graphene Oxide Hydrogels: From Reaction Products to Hydrogel Properties. Chemistry of Materials 2016, 28, 1756-1768.). Copyright (2016) American Chemical Society.

	electrical conductivity (mS/cm)	elastic modulus (kPa)	yield strength (kPa)
GHG-N-0	4.4 ± 0.1	370 ± 254	33 ± 9
GHG-N-60	3.8 ± 0.2	231 ± 81	16 ± 2
GHG-N-170	2.7 ± 0.2	225 ± 127	12 ± 1
GHG-N-290	2.8 ± 0.2	192 ± 60	14 ± 3

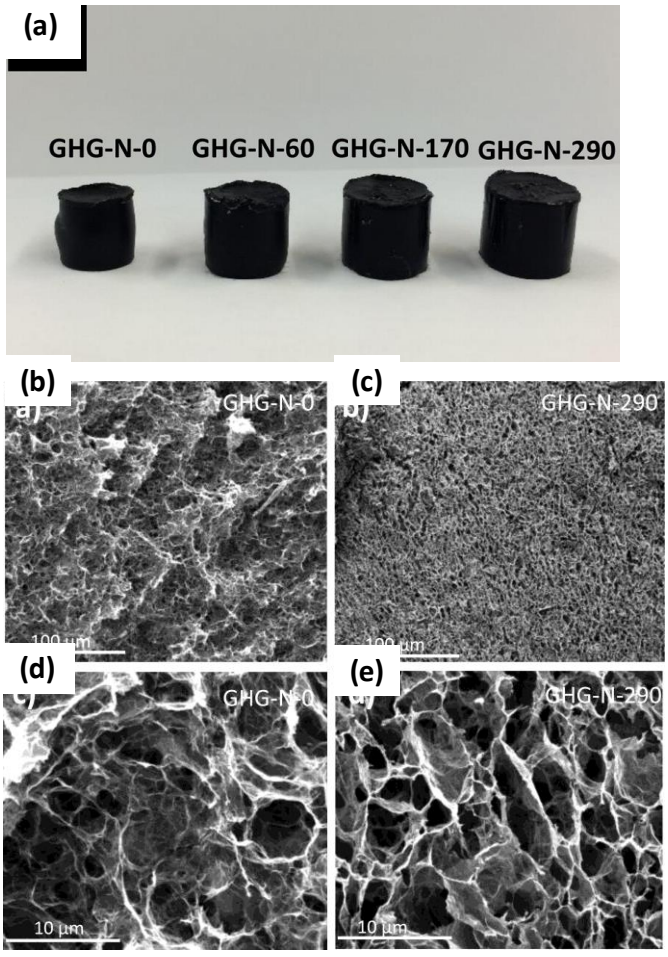

Figure 23: Images of graphene hydrogels with different ammonia content (a) As-prepared GHGs after hydrothermal reduction. (b, d) SEM images of GHG-N-0. (c, e) GHG-N-290. Reprinted with permission from ref. [8] (Hu, K.; Xie, X.; Szkopek, T.; Cerruti, M. Understanding Hydrothermally Reduced Graphene Oxide Hydrogels: From Reaction Products to Hydrogel Properties. Chemistry of Materials 2016, 28, 1756-1768.). Copyright (2016) American Chemical Society.

Graphene Aerogels (GAs) are known for their outstanding compression-tolerant and low-density as discussed in section 3.2.2. It is worth considering that compressibility and capacitance performance of GAs are conflicting, suggested by Hong *et al.*[101] In other words, a single GA cannot have both durability onto compression and capacity or capacitance. Although there are recent studies reporting GA electrodes with their extraordinary compressible performance, this is obtained at the cost of capacitance. Highly elastic GAs have been achieved by maximizing π–π interaction,[82,112] and by ordered architecture like a cellular form.[113-115] These GAs are highly dense structure while having compressive-tolerant feature. It is hard for them to have good accessibility for electrolyte ions to storage sites.[116] This results in decreased specific capacitance value. On the contrary, GA with porous and low-density structure show higher capacity because their intrinsic texture offers facile route for ion access, however, they can be easily collapsed under compressive deformation and lose their energy managing functions.

7. CONCLUSION

Studies exploring graphene-based electrodes can be categorized in to following groups: 1) Studies focused on preventing agglomeration of graphene nanosheets 2) Studies trying to retain interlayer spacing between graphene sheets by employing or particle insertion or crosslinking agents 3) Developing design strategies to enhance either the mechanical or electrochemical property, while minimizing the consequences of the other 4) Finding desirable application considering its advantages and disadvantages.

Graphene-based electrodes can be processed and combined with another component to fulfill different requirements (compressibility, flexibility, stiffness, strength, toughness, stretchability) for multifunctional applications. In this context, several benefits of 3D porous graphene hydrogels as electrode materials were presented; 1) Restacking issue of graphene sheets is minimized, due to enlarged interlayer spaces. 2) High ion diffusion, and good electrical conductivity and capacitance performance can be achieved 3) GHs can be directly used as binder-free electrodes 4) The obtained high shear storage modulus indicates that the material has good elastic response. However, they face challenges of low tensile stiffness and low strength, which is favorable features of paper-like graphene electrodes. Our recent approach explains that GO gels with ANFs addition through sol-gel approach can be detrimental to the shear storage modulus. This can be a direct consequence of ANFs preventing crosslinking between GO nanosheets by forming hydrogen bonding with GO nanosheets.

Comparative studies on graphene-based electrodes suggest that paper-like electrodes can bear mechanical load due to their management of high strength and energy and power performance simultaneously. In contrast to this, gels show rather high strain-to-failure when compared with graphene paper electrodes. They can be a recommended electrode material in the need of compression of the gels when maintaining the structural integrity is crucial under the deformations.

REFERENCES

(1) Meyvis, T. K. L.; Stubbe, B. G.; Van Steenbergen, M. J.; Hennink, W. E.; De Smedt, S. C.; Demeester, J. A comparison between the use of dynamic mechanical analysis and oscillatory shear rheometry for the characterisation of hydrogels. *International Journal of Pharmaceutics* **2002**, *244*, 163-168.

(2) Long, J. W.; Bélanger, D.; Brousse, T.; Sugimoto, W.; Sassin, M. B.; Crosnier, O. Asymmetric electrochemical capacitors—Stretching the limits of aqueous electrolytes. *MRS Bulletin* **2011**, *36*, 513-522.

(3) González, C.; Vilatela, J. J.; Molina-Aldareguia, J.; Lopes, C. s.; Llorca, J.: *Structural composites for multifunctional applications: Current challenges and Future trends*, 2017; Vol. 89.

(4) El-Kady, M. Graphene Supercapacitors: Charging Up the Future. University of California, Los Angeles, 2013.

(5) Qian, H.; Kucernak, A. R.; Greenhalgh, E. S.; Bismarck, A.; Shaffer, M. S. P. Multifunctional Structural Supercapacitor Composites Based on Carbon Aerogel Modified High Performance Carbon Fiber Fabric. *ACS Applied Materials & Interfaces* **2013**, *5*, 6113-6122.

(6) Harris, K. D.; Elias, A. L.; Chung, H. J. Flexible electronics under strain: a review of mechanical characterization and durability enhancement strategies. *Journal of Materials Science* **2016**, *51*, 2771-2805.

(7) Oyen, M. L. Mechanical characterisation of hydrogel materials. *International Materials Reviews* **2014**, *59*, 44-59.

(8) Hu, K.; Xie, X.; Szkopek, T.; Cerruti, M. Understanding Hydrothermally Reduced Graphene Oxide Hydrogels: From Reaction Products to Hydrogel Properties. *Chemistry of Materials* **2016**, *28*, 1756-1768.

(9) Kwon, S. R.; Harris, J.; Zhou, T.; Loufakis, D.; Boyd, J. G.; Lutkenhaus, J. L. Mechanically Strong Graphene/Aramid Nanofiber Composite Electrodes for Structural Energy and Power. *ACS Nano* **2017**, *11*, 6682-6690.

(10) Wu, X.-L.; Xu, A.-W. Carbonaceous hydrogels and aerogels for supercapacitors. *Journal of Materials Chemistry A* **2014**, *2*, 4852-4864.

(11) Gaikwad, A. M.; Arias, A. C. Understanding the Effects of Electrode Formulation on the Mechanical Strength of Composite Electrodes for Flexible Batteries. *ACS Applied Materials & Interfaces* **2017**, *9*, 6390-6400.

(12) Winter, M.; Brodd, R. J. What Are Batteries, Fuel Cells, and Supercapacitors? *Chemical Reviews* **2004**, *104*, 4245-4270.

(13) Parviz, D.; Irin, F.; Shah, S. A.; Das, S.; Sweeney, C. B.; Green, M. J. Challenges in Liquid-Phase Exfoliation, Processing, and Assembly of Pristine Graphene. *Advanced Materials* **2016**, *28*, 8796-8818.

(14) Bisson, A.; Rigacci, A.; Lecomte, D.; Rodier, E.; Achard, P. Drying of Silica Gels to Obtain Aerogels:Phenomenology and Basic Techniques. *Drying Technology* **2003**, *21*, 593-628.

(15) Shirshova, N.; Qian, H.; Shaffer, M. S. P.; Steinke, J. H. G.; Greenhalgh, E. S.; Curtis, P. T.; Kucernak, A.; Bismarck, A. Structural composite supercapacitors. *Composites Part A: Applied Science and Manufacturing* **2013**, *46*, 96-107.

(16) Sheng, K.-x.; Xu, Y.-x.; Li, C.; Shi, G.-q. High-performance self-assembled graphene hydrogels prepared by chemical reduction of graphene oxide. *New Carbon Materials* **2011**, *26*, 9-15.

(17) Wen, Y.; Rufford Thomas, E.; Hulicova-Jurcakova, D.; Wang, L. Nitrogen and Phosphorous Co-Doped Graphene Monolith for Supercapacitors. *ChemSusChem* **2016**, *9*, 513-520.

(18) Dikin, D. A.; Stankovich, S.; Zimney, E. J.; Piner, R. D.; Dommett, G. H. B.; Evmenenko, G.; Nguyen, S. T.; Ruoff, R. S. Preparation and characterization of graphene oxide paper. *Nature* **2007**, *448*, 457.

(19) Yang, X.; Zhu, J.; Qiu, L.; Li, D. Bioinspired Effective Prevention of Restacking in Multilayered Graphene Films: Towards the Next Generation of High-Performance Supercapacitors. *Advanced Materials* **2011**, *23*, 2833-2838.

(20) Europe, T. T. 2011.

(21) Snyder, J. F.; Wong, E. L.; Hubbard, C. W. Evaluation of Commercially Available Carbon Fibers, Fabrics, and Papers for Potential Use in Multifunctional Energy Storage Applications. *Journal of The Electrochemical Society* **2009**, *156*, A215-A224.

(22) Senokos, E.; Reguero, V.; Palma, J.; Vilatela, J. J.; Marcilla, R. Macroscopic fibres of CNTs as electrodes for multifunctional electric double layer capacitors: from quantum capacitance to device performance. *Nanoscale* **2016**, *8*, 3620-3628.

(23) Senokos, E.; Reguero, V.; Cabana, L.; Palma, J.; Marcilla, R.; Vilatela Juan, J. Large-Area, All-Solid, and Flexible Electric Double Layer Capacitors Based on CNT Fiber Electrodes and Polymer Electrolytes. *Advanced Materials Technologies* **2017**, *2*, 1600290.

(24) Meng, F.; Zhao, J.; Ye, Y.; Zhang, X.; Li, Q. Carbon nanotube fibers for electrochemical applications: effect of enhanced interfaces by an acid treatment. *Nanoscale* **2012**, *4*, 7464-7468.

(25) Basic Research Needs for Electrical Energy Storage:. https://science.energy.gov/~/media/bes/pdf/reports/files/ees_rpt_print.pdf 2017).

(26) Benson, J.; Kovalenko, I.; Boukhalfa, S.; Lashmore, D.; Sanghadasa, M.; Yushin, G. Multifunctional CNT-Polymer Composites for Ultra-Tough Structural Supercapacitors and Desalination Devices. *Advanced Materials* **2013**, *25*, 6625-6632.

(27) Han, X.; Ouyang, M.; Lu, L.; Li, J. Cycle Life of Commercial Lithium-Ion Batteries with Lithium Titanium Oxide Anodes in Electric Vehicles. *Energies* **2014**, *7*.

(28) Zhong, X. H.; Li, Y. L.; Liu, Y. K.; Qiao, X. H.; Feng, Y.; Liang, J.; Jin, J.; Zhu, L.; Hou, F.; Li, J. Y. Continuous Multilayered Carbon Nanotube Yarns. *Advanced Materials* **2009**, *22*, 692-696.

(29) Li, C.; Shi, G. Three-dimensional graphene architectures. *Nanoscale* **2012**, *4*, 5549-5563.

(30) Wu, D.; Zhang, F.; Liang, H.; Feng, X. Nanocomposites and macroscopic materials: assembly of chemically modified graphene sheets. *Chemical Society Reviews* **2012**, *41*, 6160-6177.

(31) Simon, J. R. M. a. P.: *Interface*; The Electrochemical Society: Spring, 2008; Vol. 17. pp. 31-32.

(32) Asp, L. E.; Greenhalgh, E. S. Structural power composites. *Composites Science and Technology* **2014**, *101*, 41-61.

(33) Kwon, K. H., Choi, Jong In: *The Analysis of Failure Causes on Technology Venture : A Start-up case of the Government Research Institute(GRI)*; Korean Society of Business Venturing, 2015.

(34) Wang, G.; Zhang, L.; Zhang, J. A review of electrode materials for electrochemical supercapacitors. *Chemical Society Reviews* **2012**, *41*, 797-828.

(35) Wu, Z.-S.; Zhou, G.; Yin, L.-C.; Ren, W.; Li, F.; Cheng, H.-M. Graphene/metal oxide composite electrode materials for energy storage. *Nano Energy* **2012**, *1*, 107-131.

(36) Peigney, A.; Laurent, C.; Flahaut, E.; Bacsa, R. R.; Rousset, A. Specific surface area of carbon nanotubes and bundles of carbon nanotubes. *Carbon* **2001**, *39*, 507-514.

(37) Balandin, A. A.; Ghosh, S.; Bao, W.; Calizo, I.; Teweldebrhan, D.; Miao, F.; Lau, C. N. Superior Thermal Conductivity of Single-Layer Graphene. *Nano Letters* **2008**, *8*, 902-907.

(38) Lee, C.; Wei, X.; Kysar, J. W.; Hone, J. Measurement of the Elastic Properties and Intrinsic Strength of Monolayer Graphene. *Science* **2008**, *321*, 385.

(39) Xia, J.; Chen, F.; Li, J.; Tao, N. Measurement of the quantum capacitance of graphene. *Nature Nanotechnology* **2009**, *4*, 505.

(40) Zhu, Y.; Murali, S.; Cai, W.; Li, X.; Suk Ji, W.; Potts Jeffrey, R.; Ruoff Rodney, S. Graphene and Graphene Oxide: Synthesis, Properties, and Applications. *Advanced Materials* **2010**, *22*, 3906-3924.

(41) Papageorgiou, D. G.; Kinloch, I. A.; Young, R. J. Mechanical properties of graphene and graphene-based nanocomposites. *Progress in Materials Science* **2017**, *90*, 75-127.

(42) Hummers, W. S.; Offeman, R. E. Preparation of Graphitic Oxide. *Journal of the American Chemical Society* **1958**, *80*, 1339-1339.

(43) Szabó, T.; Berkesi, O.; Forgó, P.; Josepovits, K.; Sanakis, Y.; Petridis, D.; Dékány, I. Evolution of Surface Functional Groups in a Series of Progressively Oxidized Graphite Oxides. *Chemistry of Materials* **2006**, *18*, 2740-2749.

(44) Bourlinos, A. B.; Gournis, D.; Petridis, D.; Szabó, T.; Szeri, A.; Dékány, I. Graphite Oxide: Chemical Reduction to Graphite and Surface Modification with Primary Aliphatic Amines and Amino Acids. *Langmuir* **2003**, *19*, 6050-6055.

(45) Shin, H. J.; Kim Ki, K.; Benayad, A.; Yoon, S. M.; Park Hyeon, K.; Jung, I. S.; Jin Mei, H.; Jeong, H. K.; Kim Jong, M.; Choi, J. Y.; Lee Young, H. Efficient Reduction of Graphite Oxide by Sodium Borohydride and Its Effect on Electrical Conductance. *Advanced Functional Materials* **2009**, *19*, 1987-1992.

(46) Wang, S.; Chia, P. J.; Chua, L. L.; Zhao, L. H.; Png, R. Q.; Sivaramakrishnan, S.; Zhou, M.; Goh Roland, G. S.; Friend Richard, H.; Wee Andrew, T. S.; Ho Peter, K. H. Band-like Transport in Surface-Functionalized Highly Solution-Processable Graphene Nanosheets. *Advanced Materials* **2008**, *20*, 3440-3446.

(47) Singh, V.; Joung, D.; Zhai, L.; Das, S.; Khondaker, S. I.; Seal, S. Graphene based materials: Past, present and future. *Progress in Materials Science* **2011**, *56*, 1178-1271.

(48) Wei, Y.; Sun, Z. Liquid-phase exfoliation of graphite for mass production of pristine few-layer graphene. *Current Opinion in Colloid & Interface Science* **2015**, *20*, 311-321.

(49) Yi, M.; Shen, Z. A review on mechanical exfoliation for the scalable production of graphene. *Journal of Materials Chemistry A* **2015**, *3*, 11700-11715.

(50) Paton, K. R.; Varrla, E.; Backes, C.; Smith, R. J.; Khan, U.; O'Neill, A.; Boland, C.; Lotya, M.; Istrate, O. M.; King, P.; Higgins, T.; Barwich, S.; May, P.; Puczkarski, P.; Ahmed, I.; Moebius, M.; Pettersson, H.; Long, E.; Coelho, J.; O'Brien, S. E.; McGuire, E. K.; Sanchez, B. M.; Duesberg, G. S.; McEvoy, N.; Pennycook, T. J.; Downing, C.; Crossley, A.; Nicolosi, V.; Coleman, J. N. Scalable production of large quantities of defect-free few-layer graphene by shear exfoliation in liquids. *Nature Materials* **2014**, *13*, 624.

(51) Halbig, C. E.; Nacken, T. J.; Walter, J.; Damm, C.; Eigler, S.; Peukert, W. Quantitative investigation of the fragmentation process and defect density evolution of oxo-functionalized graphene due to ultrasonication and milling. *Carbon* **2016**, *96*, 897-903.

(52) Lv, Y.; Yu, L.; Jiang, C.; Chen, S.; Nie, Z. Synthesis of graphene nanosheet powder with layer number control via a soluble salt-assisted route. *RSC Advances* **2014**, *4*, 13350-13354.

(53) El-Kady, M. F.; Shao, Y.; Kaner, R. B. Graphene for batteries, supercapacitors and beyond. *Nature Reviews Materials* **2016**, *1*, 16033.

(54) Materials Challenges Facing Electrical Energy Storage. https://www.mtixtl.com/documents/paper.pdf.

(55) He, S.; Chen, W. 3D graphene nanomaterials for binder-free supercapacitors: scientific design for enhanced performance. *Nanoscale* **2015**, *7*, 6957-6990.

(56) Frackowiak, E. Carbon materials for supercapacitor application. *Physical Chemistry Chemical Physics* **2007**, *9*, 1774-1785.

(57) Frackowiak, E.; Béguin, F. Carbon materials for the electrochemical storage of energy in capacitors. *Carbon* **2001**, *39*, 937-950.

(58) Jagannathan, S.; Liu, T.; Kumar, S. Pore size control and electrochemical capacitor behavior of chemically activated polyacrylonitrile – Carbon nanotube composite films. *Composites Science and Technology* **2010**, *70*, 593-598.

(59) Kyotani, T. Control of pore structure in carbon. *Carbon* **2000**, *38*, 269-286.

(60) Noked, M.; Soffer, A.; Aurbach, D. The electrochemistry of activated carbonaceous materials: past, present, and future. *Journal of Solid State Electrochemistry* **2011**, *15*, 1563.

(61) Pandolfo, A. G.; Hollenkamp, A. F. Carbon properties and their role in supercapacitors. *Journal of Power Sources* **2006**, *157*, 11-27.

(62) Pollak, E. Review on Engineering and Characterization of Activated Carbon Electrodes for Electrochemical Double Layer Capacitors and Separation Processes. *Israel Journal of Chemistry* **2008**, *48*, 287-303.

(63) Zhang, L. L.; Zhao, X. S. Carbon-based materials as supercapacitor electrodes. *Chemical Society Reviews* **2009**, *38*, 2520-2531.

(64) Borenstein, A.; Hanna, O.; Attias, R.; Luski, S.; Brousse, T.; Aurbach, D. Carbon-based composite materials for supercapacitor electrodes: a review. *Journal of Materials Chemistry A* **2017**, *5*, 12653-12672.

(65) Kossyrev, P. Carbon black supercapacitors employing thin electrodes. *Journal of Power Sources* **2012**, *201*, 347-352.

(66) Activated Carbon Basics. http://www.haycarb.com/activated-carbon.

(67) Lee, J.; Kim, J.; Hyeon, T. Recent Progress in the Synthesis of Porous Carbon Materials. *Advanced Materials* **2006**, *18*, 2073-2094.

(68) Simon, P.; Gogotsi, Y. Materials for electrochemical capacitors. *Nature Materials* **2008**, *7*, 845.

(69) Hall, P. J.; Mirzaeian, M.; Fletcher, S. I.; Sillars, F. B.; Rennie, A. J. R.; Shitta-Bey, G. O.; Wilson, G.; Cruden, A.; Carter, R. Energy storage in electrochemical capacitors: designing functional materials to improve performance. *Energy & Environmental Science* **2010**, *3*, 1238-1251.

(70) Castro Neto, A. H.; Guinea, F.; Peres, N. M. R.; Novoselov, K. S.; Geim, A. K. The electronic properties of graphene. *Reviews of Modern Physics* **2009**, *81*, 109-162.

(71) Structural Power Technology Turns Car Doors into Batteries. https://www.extremetech.com/extreme/84316-structural-power-technology-turns-car-doors-into-batteries.

(72) Multifunctional composite materials for energy storage in structural load paths. https://arpa-e.energy.gov/sites/default/files/documents/files/CSESS%20Asp.pdf.

(73) O'Brien, D. J.; Baechle, D. M.; Wetzel, E. D. Design and performance of multifunctional structural composite capacitors. *Journal of Composite Materials* **2011**, *45*, 2797-2809.

(74) F. Snyder, J.; L. Wong, E.; W. Hubbard, C.: *Evaluation of Commercially Available Carbon Fibers, Fabrics, and Papers for Potential Use in Multifunctional Energy Storage Applications*, 2009; Vol. 156.

(75) Gao, Y. Graphene and Polymer Composites for Supercapacitor Applications: a Review. *Nanoscale Research Letters* **2017**, *12*, 387.

(76) El-Kady, M. F.; Strong, V.; Dubin, S.; Kaner, R. B. Laser Scribing of High-Performance and Flexible Graphene-Based Electrochemical Capacitors. *Science* **2012**, *335*, 1326.

(77) Yan, J.; Wei, T.; Shao, B.; Ma, F.; Fan, Z.; Zhang, M.; Zheng, C.; Shang, Y.; Qian, W.; Wei, F. Electrochemical properties of graphene nanosheet/carbon black composites as electrodes for supercapacitors. *Carbon* **2010**, *48*, 1731-1737.

(78) Xu, Y.; Sheng, K.; Li, C.; Shi, G. Self-assembled graphene hydrogel via a one-step hydrothermal process. *Acs Nano* **2010**, *4*, 4324.

(79) *Nanomaterials in Advanced Batteries and Supercapacitors*; Springer, 2016

(80) Lv, W.; Zhang, C.; Li, Z.; Yang, Q.-H. Self-Assembled 3D Graphene Monolith from Solution. *The Journal of Physical Chemistry Letters* **2015**, *6*, 658-668.

(81) Goldstein, A. P.; Mickelson, W.; Machness, A.; Lee, G.; Worsley, M. A.; Woo, L.; Zettl, A. Simultaneous Sheet Cross-Linking and Deoxygenation in the Graphene Oxide Sol–Gel Transition. *The Journal of Physical Chemistry C* **2014**, *118*, 28855-28860.

(82) Li, Y.; Chen, J.; Huang, L.; Li, C.; Hong, J. D.; Shi, G. Highly Compressible Macroporous Graphene Monoliths via an Improved Hydrothermal Process. *Advanced Materials* **2014**, *26*, 4789-4793.

(83) Zhang, X.; Sui, Z.; Xu, B.; Yue, S.; Luo, Y.; Zhan, W.; Liu, B. Mechanically strong and highly conductive graphene aerogel and its use as electrodes for electrochemical power sources. *Journal of Materials Chemistry* **2011**, *21*, 6494-6497.

(84) Worsley, M. A.; Pauzauskie, P. J.; Olson, T. Y.; Biener, J.; Satcher, J. H.; Baumann, T. F. Synthesis of Graphene Aerogel with High Electrical Conductivity. *Journal of the American Chemical Society* **2010**, *132*, 14067-14069.

(85) Cheng, Y.; Zhou, S.; Hu, P.; Zhao, G.; Li, Y.; Zhang, X.; Han, W. Enhanced mechanical, thermal, and electric properties of graphene aerogels via supercritical ethanol drying and high-temperature thermal reduction. *Scientific Reports* **2017**, *7*, 1439.

(86) Şahin, İ.; Özbakır, Y.; İnönü, Z.; Ulker, Z.; Erkey, C. Kinetics of Supercritical Drying of Gels. *Gels* **2018**, *4*.

(87) Normand, V.; Lootens, D. L.; Amici, E.; Plucknett, K. P.; Aymard, P. New Insight into Agarose Gel Mechanical Properties. *Biomacromolecules* **2000**, *1*, 730-738.

(88) Tse, J. R.; Engler, A. J.: Preparation of Hydrogel Substrates with Tunable Mechanical Properties. In *Current Protocols in Cell Biology*; John Wiley & Sons, Inc., 2001.

(89) Roberts Justine, J.; Earnshaw, A.; Ferguson Virginia, L.; Bryant Stephanie, J. Comparative study of the viscoelastic mechanical behavior of agarose and poly(ethylene glycol) hydrogels. *Journal of Biomedical Materials Research Part B: Applied Biomaterials* **2011**, *99B*, 158-169.

(90) Gu, W. Y.; Yao, H.; Huang, C. Y.; Cheung, H. S. New insight into deformation-dependent hydraulic permeability of gels and cartilage, and dynamic behavior of agarose gels in confined compression. *Journal of Biomechanics* **2003**, *36*, 593-598.

(91) http://files.hanser.de/hanser/docs/20041012_2411215439-82_3-446-22673-7.pdf.

(92) Macosko, C. W.: *Rheology: Principles, Measurements and Applications*; VCH Publishers, 1994.

(93) Son, B.; Ryou, M.-H.; Choi, J.; Lee, T.; Yu, H. K.; Kim, J. H.; Lee, Y. M. Measurement and Analysis of Adhesion Property of Lithium-Ion Battery Electrodes with SAICAS. *ACS Applied Materials & Interfaces* **2014**, *6*, 526-531.

(94) Haselrieder, W.; Westphal, B.; Bockholt, H.; Diener, A.; Höft, S.; Kwade, A. Measuring the coating adhesion strength of electrodes for lithium-ion batteries. *International Journal of Adhesion and Adhesives* **2015**, *60*, 1-8.

(95) Burnett, P. J.; Rickerby, D. S. The relationship between hardness and scratch adhesion. *Thin Solid Films* **1987**, *154*, 403-416.

(96) Chen, J.; Liu, J.; Qi, Y.; Sun, T.; Li, X. Unveiling the Roles of Binder in the Mechanical Integrity of Electrodes for Lithium-Ion Batteries. *Journal of The Electrochemical Society* **2013**, *160*, A1502-A1509.

(97) Gogotsi, Y.; Simon, P. True Performance Metrics in Electrochemical Energy Storage. *Science* **2011**, *334*, 917.

(98) Tan, R. K. L.; Reeves, S. P.; Hashemi, N.; Thomas, D. G.; Kavak, E.; Montazami, R.; Hashemi, N. N. Graphene as a flexible electrode: review of fabrication approaches. *Journal of Materials Chemistry A* **2017**, *5*, 17777-17803.

(99) Mendoza-Sánchez, B.; Gogotsi, Y. Synthesis of Two-Dimensional Materials for Capacitive Energy Storage. *Advanced Materials* **2016**, *28*, 6104-6135.

(100) Tang, H.; Gao, P.; Bao, Z.; Zhou, B.; Shen, J.; Mei, Y.; Wu, G. Conductive resilient graphene aerogel via magnesiothermic reduction of graphene oxide assemblies. *Nano Research* **2015**, *8*, 1710-1717.

(101) Hong, J. Y.; Bak Bo, M.; Wie Jeong, J.; Kong, J.; Park Ho, S. Reversibly Compressible, Highly Elastic, and Durable Graphene Aerogels for Energy Storage Devices under Limiting Conditions. *Advanced Functional Materials* **2014**, *25*, 1053-1062.

(102) Zhao, Y.; Hu, C.; Hu, Y.; Cheng, H.; Shi, G.; Qu, L. A Versatile, Ultralight, Nitrogen-Doped Graphene Framework. *Angewandte Chemie International Edition* **2012**, *51*, 11371-11375.

(103) Rodriguez-Perez, L.; Herranz, M. a. A.; Martin, N. The chemistry of pristine graphene. *Chemical Communications* **2013**, *49*, 3721-3735.

(104) Hirsch, A.; Englert, J. M.; Hauke, F. Wet Chemical Functionalization of Graphene. *Accounts of Chemical Research* **2013**, *46*, 87-96.

(105) Liu, J.; Tang, J.; Gooding, J. J. Strategies for chemical modification of graphene and applications of chemically modified graphene. *Journal of Materials Chemistry* **2012**, *22*, 12435-12452.

(106) Zhu, C.; Zhai, J.; Dong, S. Ionic liquid-induced three-dimensional macroassembly of graphene and its applications in electrochemical energy storage. *Nanoscale* **2014**, *6*, 10077-10083.

(107) Georgakilas, V.; Otyepka, M.; Bourlinos, A. B.; Chandra, V.; Kim, N.; Kemp, K. C.; Hobza, P.; Zboril, R.; Kim, K. S. Functionalization of Graphene: Covalent and Non-Covalent Approaches, Derivatives and Applications. *Chemical Reviews* **2012**, *112*, 6156-6214.

(108) Lee, W. J.; Maiti, U. N.; Lee, J. M.; Lim, J.; Han, T. H.; Kim, S. O. Nitrogen-doped carbon nanotubes and graphene composite structures for energy and catalytic applications. *Chemical Communications* **2014**, *50*, 6818-6830.

(109) Chen, P.; Yang, J.-J.; Li, S.-S.; Wang, Z.; Xiao, T.-Y.; Qian, Y.-H.; Yu, S.-H. Hydrothermal synthesis of macroscopic nitrogen-doped graphene hydrogels for ultrafast supercapacitor. *Nano Energy* **2013**, *2*, 249-256.

(110) Ma, J.; Sun, Y.; Zhang, M.; Yang, M.; Gong, X.; Yu, F.; Zheng, J. Comparative Study of Graphene Hydrogels and Aerogels Reveals the Important Role of Buried Water in Pollutant Adsorption. *Environmental Science & Technology* **2017**, *51*, 12283-12292.

(111) Xu, Y.; Sheng, K.; Li, C.; Shi, G. Self-Assembled Graphene Hydrogel via a One-Step Hydrothermal Process. *ACS Nano* **2010**, *4*, 4324-4330.

(112) Li, C.; Shi, G. Functional Gels Based on Chemically Modified Graphenes. *Advanced Materials* **2014**, *26*, 3992-4012.

(113) Huang, H.; Chen, P.; Zhang, X.; Lu, Y.; Zhan, W. Edge-to-Edge Assembled Graphene Oxide Aerogels with Outstanding Mechanical Performance and Superhigh Chemical Activity. *Small* **2013**, *9*, 1397-1404.

(114) Hu, C.; Zhai, X.; Liu, L.; Zhao, Y.; Jiang, L.; Qu, L. Spontaneous Reduction and Assembly of Graphene oxide into Three-Dimensional Graphene Network on Arbitrary Conductive Substrates. *Scientific Reports* **2013**, *3*, 2065.

(115) Xie, X.; Zhou, Y.; Bi, H.; Yin, K.; Wan, S.; Sun, L. Large-range Control of the Microstructures and Properties of Three-dimensional Porous Graphene. *Scientific Reports* **2013**, *3*, 2117.

(116) Li, P.; Kong, C.; Shang, Y.; Shi, E.; Yu, Y.; Qian, W.; Wei, F.; Wei, J.; Wang, K.; Zhu, H.; Cao, A.; Wu, D. Highly deformation-tolerant carbon nanotube sponges as supercapacitor electrodes. *Nanoscale* **2013**, *5*, 8472-8479.

APPENDIX

SUMMARY OF ELECTROCHEMICAL AND MECHANICAL PROPERTIES OF CARBON-BASED ELECTRODES*

Type of fiber	**Specific strength (GPa/SG)**	**Specific modulus (GPa/SG)**	**Energy to break (J/g)**	**Compression strength (GPa/SG)**	**Capacitance (F/g)**	**Reference**
HTA carbon fiber + carbon aerogel	–	–	–	–	6–14	[2,5]
HTA carbon fiber	2.2	135	18.6	–	0.06	[5,20]
AS4 carbon fiber	2.4	127	22.4	1.4	1.3	[21]
CNT fiber	0.9	44	30	0.6	42	[22]
CNT fiber	2	100	75	0.6	33	[23]
Functionalised-CNT fiber	1.5	50	18		50–75	[24]
CNT fiber	0.15	10	8.625	–	23	[26]
CNT fiber	0.75	30	92	0.6	79.8	[28]

Mechanical properties are normalized by specific gravity (SG)

*Reprinted with permission from *Structural Composites for Multifunctional Applications: Current Challenges and Future Trends*, González, C.; Vilatela, J. J.; Molina-Aldareguia, J.; Lopes, C. s.; Llorca, J.:, 2017; Vol. 89.